



**THE EFFECT OF MICROSTRUCTURE ON TO ER308L Si WAAM  
STRUCTURE USING INOCULANT**

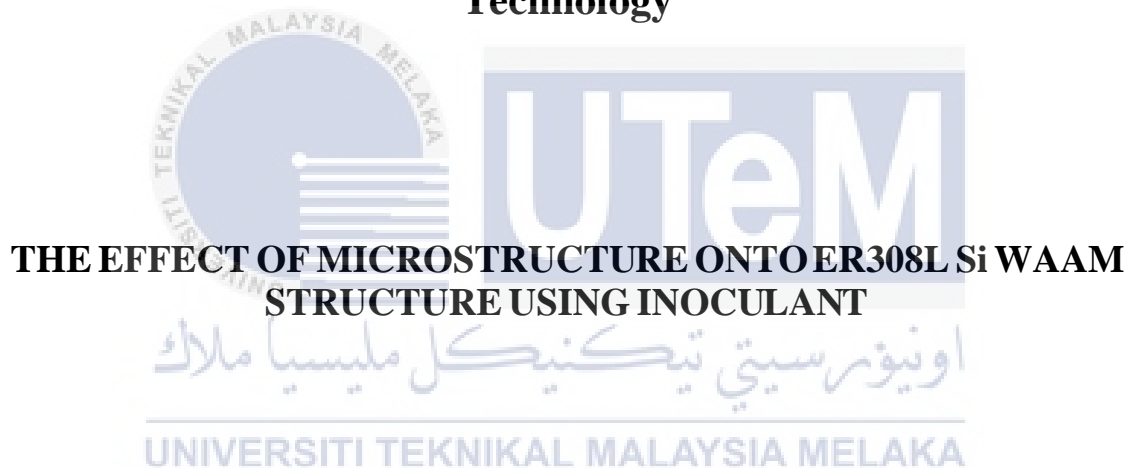


**BACHELOR OF MECHANICAL ENGINEERING TECHNOLOGY  
(AUTOMOTIVE TECHNOLOGY) WITH HONOURS**

**2023**



**Faculty of Mechanical and Manufacturing Engineering  
Technology**



**THE EFFECT OF MICROSTRUCTURE ONTO ER308L Si WAAM  
STRUCTURE USING INOCULANT**

**Shahrul Helmi Bin Lasemin**

**Bachelor of Mechanical Engineering Technology (Automotive Technology) with  
Honours**

**2023**

**THE EFFECT OF MICROSTRUCTURE ONTO ER308L Si WAAM STRUCTURE  
USING INOCULANT**

**SHAHRUL HELMI BIN LASEMIN**

**A thesis submitted  
in fulfillment of the requirements for the degree of  
Bachelor of Mechanical Engineering Technology (Automotive Technology) with  
Honours**



**Faculty of Mechanical and Manufacturing Engineering Technology**

**UNIVERSITI TEKNIKAL MALAYSIA MELAKA**

**UNIVERSITI TEKNIKAL MALAYSIA MELAKA**

**2023**

## DECLARATION

I declare that this Choose an item. entitled “Microstructure of 3D Printed Structure Produced Using Metal Additive Manufacturing with Wire Arc Robotic System” is the result of my own research except as cited in the references. The Choose an item. has not been accepted for any degree and is not concurrently submitted in candidature of any other degree.

Signature

:



Name

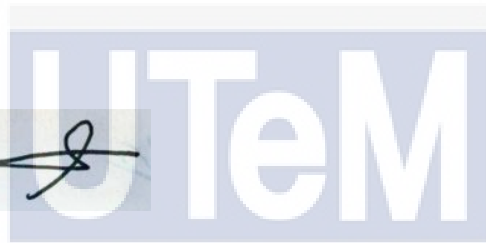
:

SHAHRUL HELMI BIN LASEMIN

Date

:

10.01.2023



UNIVERSITI TEKNIKAL MALAYSIA MELAKA

## APPROVAL

I hereby declare that I have checked this thesis and in my opinion, this thesis is adequate in terms of scope and quality for the award of the Bachelor of Mechanical Engineering Technology (Automotive Technology) with Honours.

Signature :



**TS. MOHD HAJRIZAL BIN OSMAN**  
Pensyarah  
Jabatan Teknologi Industri  
Fakulti Teknologi Kejuruteraan Mekanikal Dan Pembuatan  
Universiti Teknikal Malaysia Melaka

Supervisor Name : TS. MOHD HAJRIZAL BIN OSMAN

Date : 10.01.2023

اونيورسيٲي تيكنيكل مليسيا ملاك  
UNIVERSITI TEKNIKAL MALAYSIA MELAKA

## DEDICATION

To my family.



## ABSTRACT

Additive manufacturing (AM)/3D printing is a new manufacturing process that expands the creative possibilities available to product designers. These last several years have seen a rise in the popularity of materials based on metal. An end result is achieved by serially applying thin layers of material. Thus, the entire process of creating new products is greatly accelerated. However, the technology is still immature and cannot fully replace existing methods due to its subpar mechanical properties. Furthermore, the cost of using a laser to create commercial 3D metal prints is very high. MIG, or metal inert gas, is a viable replacement that saves money and resources (MIG). Additive manufacturing with MIG welders involves the use of high-temperature materials and processes, hence this study will examine the interplay between materials and heat (MIG-WAAM). When printing in metal, each layer must go through a process of heating, cooling, hardening, and reheating. In other words, we need to know how the layers interact with one another and the environment before we can construct a 3D object using a melt pool and a single-track mechanism and mixing with Alumina Oxide and Titanium Carbide Powder. Many temperature-measuring instruments, such as pyrometers and thermal cameras, as well as high-speed cameras, will be used to keep an eye on the process as it unfolds. Dimensional accuracy, microstructure, the heat affected zone (HAZ), hardness, and porosity are just few of the physical phenomena that are intended to be studied in relation to processes. The Response Surface Methodology will be used to establish a connection between the imaging system's recorded physical events and the pyrometer's readings (RSM). Geomagic software and coordinate measuring equipment will be used to compare the CAD and printed structures, taking into account all relevant parameters and melt pool behaviour (CMM). The future of porosity calculations lies on Archimedes' Principles. Last but not least, we'll be doing static strength tests in accordance with ASTM E8M-04. This will aid in the study of the correlation between the qualities of the 3D structure process and the properties of the wire arc robotic system while making metal additively. i)The surface quality of the wall and the accumulation efficiency both increased despite the fact that the wire feeding speed remained unchanged and the amount of heat input and alumina oxide and titanium carbide paste remained unchanged. The microstructure is similar to that of stainless steel, but the combined strength of alumina carbide and titanium oxide makes the material far more formidable than stainless steel alone.

## ***ABSTRAK***

Pembuatan tambahan (AM)/Pencetakan 3D ialah proses pembuatan baharu yang meluaskan kemungkinan kreatif yang tersedia untuk pereka produk. Beberapa tahun kebelakangan ini telah menyaksikan peningkatan dalam populariti bahan berasaskan logam. Hasil akhir dicapai dengan menggunakan lapisan nipis bahan secara bersiri. Oleh itu, keseluruhan proses mencipta produk baru sangat dipercepatkan. Walau bagaimanapun, teknologi itu masih belum matang dan tidak dapat menggantikan sepenuhnya kaedah sedia ada kerana sifat mekanikalnya yang rendah. Tambahan pula, kos penggunaan laser untuk mencipta cetakan logam 3D komersial adalah sangat tinggi. MIG, atau gas lengai logam, ialah pengganti berdaya maju yang menjimatkan wang dan sumber (MIG). Pembuatan aditif dengan pengimpal MIG melibatkan penggunaan bahan dan proses suhu tinggi, justeru kajian ini akan mengkaji interaksi antara bahan dan haba (MIG-WAAM). Apabila mencetak dalam logam, setiap lapisan mesti melalui proses pemanasan, penyejukan, pengerasan, dan pemanasan semula. Dalam erti kata lain, kita perlu mengetahui cara lapisan berinteraksi antara satu sama lain dan persekitaran sebelum kita boleh membina objek 3D menggunakan kolam cair dan mekanisme trek tunggal. Banyak alat pengukur suhu, seperti pyrometer dan kamera termal, serta kamera berkelajuan tinggi, akan digunakan untuk memerhatikan proses semasa ia berlaku. Ketepatan dimensi, struktur mikro, zon terjejas haba (HAZ), kekerasan, dan keliangan hanyalah beberapa daripada fenomena fizikal yang bertujuan untuk dikaji berhubung dengan proses. Metodologi Permukaan Tindak Balas akan digunakan untuk mewujudkan hubungan antara peristiwa fizikal yang direkodkan sistem pengimejan dan bacaan pyrometer (RSM). Perisian geomagik dan peralatan pengukur koordinat akan digunakan untuk membandingkan CAD dan struktur bercetak, dengan mengambil kira semua parameter yang berkaitan dan tingkah laku kolam cair (CMM). Masa depan pengiraan keliangan terletak pada Prinsip Archimedes. Akhir sekali, kami akan melakukan ujian kekuatan statik mengikut ASTM E8M-04. Ini akan membantu dalam kajian korelasi antara kualiti proses struktur 3D dan sifat sistem robot arka dawai semasa membuat logam secara tambahan. Kualiti permukaan dinding dan kecekapan pengumpulan kedua-duanya meningkat walaupun pada hakikatnya kelajuan suapan wayar kekal tidak berubah dan jumlah input haba dan pes alumina oksida dan titanium karbida kekal tidak berubah. Struktur mikro adalah serupa dengan keluli tahan karat, tetapi kekuatan gabungan alumina karbida dan titanium oksida menjadikan bahan itu jauh lebih menggerunkan daripada keluli tahan karat sahaja.

## ACKNOWLEDGEMENTS

First, all praised to Almighty Allah for a strength given to me during completing this report. I would like to thank to my family for their support and encouragements whether it is financially or morally. I also want to express my gratitude to my supervisor, Mister TS Mohd Hairizal Bin Osman who always helping me in giving suggestions and lot of information in finishing this report. Apart of that, a huge thanks to my fellow friends in 3 BMMA S2/1 especially to Amerul Haziq, Muhammad Arif, Muhammad Alif, and Rizmanhadi who always encourage and share knowledges with me. Finally, a special thanks to the authority of Universiti Teknikal Malaysia Melaka (UTeM) for the good facilities and environment to make this experiment and this research report, especially to Faculty of Mechanical and Manufacturing Engineering Technology (FTKMP) for giving me the opportunities and chance to use the materials, apparatuses, and instruments provided in the laboratory.



## TABLE OF CONTENTS

	<b>PAGE</b>
<b>DECLARATION</b>	
<b>APPROVAL</b>	
<b>DEDICATION</b>	
<b>ABSTRACT</b>	<b>i</b>
<b>ABSTRAK</b>	<b>ii</b>
<b>ACKNOWLEDGEMENTS</b>	<b>iii</b>
<b>TABLE OF CONTENTS</b>	<b>iv</b>
<b>LIST OF TABLES</b>	<b>vii</b>
<b>LIST OF FIGURES</b>	<b>viii</b>
<b>LIST OF SYMBOLS AND ABBREVIATIONS</b>	<b>xi</b>
<b>LIST OF APPENDICES</b>	<b>xii</b>
<b>CHAPTER 1 INTRODUCTION</b>	<b>13</b>
1.1 Background	13
1.2 Problem Statement	15
1.3 Research Objective	16
1.4 Scope of Research	17
<b>CHAPTER 2 LITERATURE REVIEW</b>	<b>18</b>
2.1 Introduction	18
2.1.1 Additive Manufacturing (AM)	18
2.2 Wire Arc Manufacturing (WAAM)	20
2.3 MIG- Gas Metal Arc Welding (GMAW)	22
2.3.1 ABB WAAM Robots Welding	24
2.3.2 Welding Current	26
2.3.3 Low Carbon Steel/Mild Steel	26
2.4 Filler Wire (ER308SL)	27
2.4.1 Alumina Powder	28
2.4.2 Titanium Carbide (TIC)	29
2.4.3 Shielding Gasses for Welding	30
2.5 Optimization of Microstructure Process	33
2.5.1 Analysis Effect of Heat Input in WAAM Process	33
2.5.2 Pyrometer	33
2.6 Microstructure Characteristics of Samples	34
2.7 Microhardness Properties	38

<b>CHAPTER 3</b>	<b>METHODOLOGY</b>	<b>42</b>
3.1	Introduction	42
3.2	Flow Chart Research	42
3.3	Material Selection	44
	3.3.1 ER308L Sl Arc Wire	45
	3.3.2 Shielding Gasses (Argon + Co2 Gas)	46
	3.3.3 Mild Steel	47
	3.3.4 Alumina powder	49
	3.3.5 Titanium Carbide (TIC)	49
	3.3.6 Kalling' No. 2	50
3.4	Parameter	51
3.5	Run Experiment	52
3.6	Result Recorded	53
	3.6.1 Surface Grinding	53
	3.6.2 Milling Process	53
	3.6.3 Wire Cut Process	55
	3.6.4 Mounting Specimen process	55
	3.6.5 Polishing Process	56
	3.6.6 Etching Process	57
	3.6.7 Optical Microscopy (OM)	58
	3.6.8 Scanning Electron Microscope (SEM)	59
3.7	Equipment and Machine	59
	3.7.1 ABB Robotic Welding IRB 1410	60
	3.7.2 Milling Machine FM-16V8	62
	3.7.3 Wire Cut EDM Sodick VZ300L	64
	3.7.4 Optical Microscope	65
	3.7.5 Scanning Electron Microscope JEOL JSM-6010PLUS/LV	66
3.8	Summary	67
<b>CHAPTER 4</b>		<b>69</b>
4.1	Introduction	69
4.2	Surface Morphology of Walls	69
4.3	Porosity of Walls	70
4.4	Microstructure of Walls	71
	4.4.1 Microstructure of Walls in As-Deposited State	71
4.5	Mechanical Properties and Fracture Morphology of Walls	73
	4.5.1 Mechanical Properties of Walls	73
	4.5.2 Fracture Morphology of Walls	74
<b>CHAPTER 5</b>		<b>76</b>
5.1	Conclusions	76
5.2	Recommendation	76
<b>REFERENCES</b>		<b>78</b>
<b>APPENDICES</b>		<b>80</b>



## LIST OF TABLES

TABLE	TITLE	PAGE
Table 1	Properties of raw material	29
Table 2	Parameter of Shielding Gasses	32
Table 3	Clasification of shielding gasses for arc welding	47
Table 4	Parameter of robot welding ABB	51



## LIST OF FIGURES

FIGURE	TITLE	PAGE
Figure 1-1	Sample Preparation of WAAM process	13
Figure 1-2	TIG vs MIG Welding	14
Figure 2-1	How robots are solving the biggest challenges in welding	19
Figure 2-2	The hidden complexities of Wire Arc Additive Manufacturing	21
Figure 2-3	Diagram of WAAM process	22
Figure 2-4	Diagram of MIG process	23
Figure 2-5	Apparatus for MIG welding	24
Figure 2-6	Illustration of a robotic WAAM (Wire Arc Additive Manufacturing)	25
Figure 2-7	Apparatus and Illustration process of welding	26
Figure 2-8	Main chemical contents of feeding wires of 308SLi filler wire	27
Figure 2-9	Alumina Oxide Powder	28
Figure 2-10	Titanium Carbide	30
Figure 2-11	Illustration on how shielding gasses work	31
Figure 2-12	Flow chart of stable WAAM process	32
Figure 2-13	Pyrometer	34
Figure 2-14	Optical micrographs taken from the WAAM-ER70S-6 steel wall at the fusion line and center of the melt pool. a Higher magnification of the enclosed area in a shown by A, and the inserted image shows an example of a phase fraction analysis micrograph	36

Figure 2-15 (on the left) are macrostructures of the top and bottom halves of the overlapping wall in the transversal direction (the plane XZ), and (on the right) are microstructures of the overlapped wall.	38
Figure 2-16 Microhardness graph of a NiTi LAM b NiTi MBSM c CuAlNi	39
Figure 2-17 Microhardness samples	40
Figure 2-18 Microstructure of built materials in the upper region (a), in the middle region with lower magnification (b), the lower region (c)	41
Figure 3-1 Flow Chart methodology of the Microstructure Experiment Process	43
Figure 3-2 ER308L SI Arc Wire	45
Figure 3-3 Shielding Gasses (Argon+Co2)	47
Figure 3-4 Low carbon mild steel plate	48
Figure 3-5 The Compound of Titanium Carbide Powder	50
Figure 3-6 The High Acidic Kalling's No.2	50
Figure 3-7 Setup for fabrication process	52
Figure 3-8 Milling Process	54
Figure 3-9 On the left side, there is a picture of the wire cut process with an EDM wire-cut machine. On the right, there is a picture of a dog bone that has been cut to the right size for the next step.	55
Figure 3-10 show a Phenolic Powder (Black) Mounting Compound	56
Figure 3-11 show a condition of specimen after mounting at the left side. At the right side show a picture of polishing process using a sandpaper.	57
Figure 3-12 show the high acidic concentration Kalling	57
Figure 3-13 Optical Microscope	59
Figure 3-14 IRC5 Single Cabinet Controller	61

Figure 3-15 Kemppi KemArc Pulse 250	62
Figure 3-16 Milling Machine	63
Figure 3-17 Sodick VZ300L wire-cut machine	64
Figure 3-18 Optical Microscope	65
Figure 3-19 JEOL JSM-6010PLUS/LV SEM machine	67
Figure 4-1 Surface morphology of alumina oxide powder left side, and titanium carbide powder right side	70
Figure 4-2 Porosity of titanium carbide at the left side and the right side are the porosity of alumina powder wall.	70
Figure 4-3 Metallographs of (a) stainless steel wall and (b) alumina oxide wall, and SEM images of (C) titanium carbide wall and (D) alumina oxide wall in as-deposited state respectively.	72
Figure 4-4 Mechanical properties of printed Titanium Carbide wall	73
Figure 4-5 Mechanical properties of printed Alumina oxide wall	74
Figure 4-6 SEM images showing fracture morphology of alumina oxide and titanium carbide: (A) longitudinal of alumina oxide; (b) transverse of alumina oxide; (c) longitudinal of titanium carbide; and (d) transverse of titanium carbide.	75

## LIST OF SYMBOLS AND ABBREVIATIONS

AM	-	Additive Manufacturing
3D	-	Three Dimension
WAAM	-	Wire Arc Additive Manufacturing
GMAW	-	Gas Metal Arc Welding
%	-	Percentage
CAD	-	Computer Aided Design
	-	
	-	



## LIST OF APPENDICES

APPENDIX	TITLE	PAGE
APPENDIX 1	Turnitin Report	81



# CHAPTER 1

## INTRODUCTION

### 1.1 Background

Wire + circular segment added substance fabricating (WAAM) could be a coordinated vitality testimony (DED) strategy. Its employments an electric bend to at the same time dissolve and store metal wire onto a substrate, in this manner building up a portion layer by layer. (WAAM) has as of now demonstrated to be effective to deliver expansive metal parts. Be that as it may, there still no guidelines that available to name the quality that got to be prerequisites of the parts delivered by WAAM and this may avoid a broader selection of the strategy. Figure 1-1 show the sample preparation of WAAM process.



**Figure 1-1 Sample Preparation of WAAM process**

WAAM can be utilized to construct expansive parts rapidly, due to its higher testimony rates. It's too building near-net shape, which decreases machining operations

and a fabric wastage in comparison to a conventional fabricating strategy of machining the casting or manufacturing. Coming about in less generation costs when compared to other metal added substance fabricating (MAM) innovations. A vital step towards the quality confirmation of WAAM parts will be the advancement of dependable and inline Non-Destructive Testing (NDT) frameworks that competent of recognizing portion abandons, which is often caused by porosity or need of combination between layers. Within the later a long time, AM has been utilized to plan and fabricate of models, with the car, aviation, therapeutic businesses, and defense receiving these innovations.

TIG welding, like MIG welding, uses an electric arc. TIG welding requires the use of a tungsten electrode. Tungsten is one of the most difficult metals to work with. It will not disintegrate or burn away. Welding can be done using a fusion method that uses or does not use a filler metal. An external gas supply, such as argon or helium, is also used in TIG. TIG welding is also used in the aerospace and automotive industries, as well as other industrial areas. Welding wagon frames, fenders, and other critical equipment is also a fantastic form of welding for Iowa because it may be highly valuable for farmers. Figure 1-2 show the TIG welding vs MIG welding process.



**Figure 1-2 TIG vs MIG Welding**

Construction, maintenance, and repair, as well as underwater pipelines and industrial manufacturing, all require stick welding. This were utilised shielded metal arc welding, also known as Stick welding, for this form of welding. Utilise a disposable and well-protected electrode, such as a stick. By creating an arc between a covered metal electrode and the base metal workpiece, the stick softens and mixes metals. The stick's protective layer melts as it melts, shielding the weld region from oxygen and other gases in the air. Flux-cored arc welding is like MIG welding because both used continuous wire and power supply. A continuous electrode will be combined with a base metal. The electrode is a flux-filled hollow tube that is fed into the weld pool using the weld cannon. A flux shield protects the welder from the elements when welding outside. This technique of welding is utilised in the machining industry to join thicker metals together.

## 1.2 Problem Statement

In this research, additive manufacturing is one of the hot topics in the manufacturing and engineering worlds. This ability can create three-dimensional, complex and near net to the shape parts in a layer-by-layer deposition process were currently a major driving of force for a breakthrough. These breakthroughs were observed either in the process by itself using developing variants process with a dedicated purposes to increase capabilities, but also on the materials used, since the non-equilibrium solidification conditions which can occur during fusion-based additive manufacturing will lead to microstructural features not often found in conventional materials manufacturing process.

The fabrication is a complex shaped parts via WAAM were becoming well-establishing in both academia and industry. Most of the relevant engineering alloys

(aluminium, titanium, and steels that including stainless) have already been used in WAAM with very good results that have been prove the viability of the technique to produce a custom-made large metallic part. However, due to its destitute mechanical properties, this procedures or process isn't developed sufficient to supplant conventional procedures. One aspect that is not yet well explored concerns the possibility of using WAAM for repair applications. Some of the properties that were related to this method was porosity, cracking, residual stress, and deformity. Some defect on a microstructure structure may occur when welding process layer by layer such as due to high temperature of the welding process. This could greatly decrease costs associated with the need to completely renew a given structural part, since the WAAM technology it is possible to perform localized repairs.

### **1.3 Research Objective**

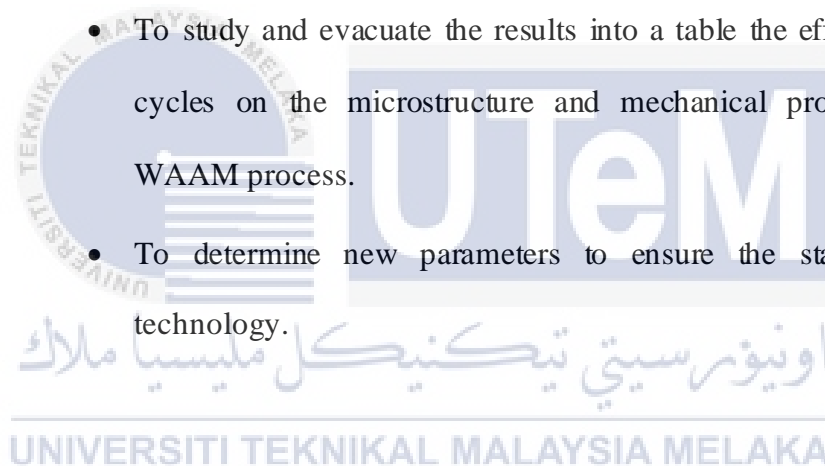
The main aim for this research is to investigate the process-properties relationship between materials and heat during MIG assisted wire arc additive manufacturing (MIG-WAAM). So, this is objectives that includes as a follows:

- a) To fabricate (WAAM) structure using wire arc robotic system.
- b) To optimize and get the optimal parameter of the process.
- c) To study the effect of microstructure on ER308L arc wire mixture with inoculant materials such as Alumina Oxide Powder and Titanium Carbait Powder.

## 1.4 Scope of Research

This research is to develop and study the process parameter of 3D printing structure procedure using a metal additive manufacturing using wire arc robotic system. The scope of this research are as follows:

- To evaluate the hardness behaviour using a micro-hardness tester, to determine the optimal parameter, and to identify the most significant parameters influencing hardness enhancement.
- To study and investigate the characteristics surface of layer by layer for improving the microstructure properties.
- To study and evaluate the results into a table the effect of thermal cycles on the microstructure and mechanical properties during WAAM process.
- To determine new parameters to ensure the stability of this technology.



## CHAPTER 2

### LITERATURE REVIEW

#### 2.1 Introduction

In this chapter, function of literature review was to be conducted to acquire the information and to develop skills that required to complete the research. These sources include a previous related reviews from the internet, journals, articles, and magazines that conclude findings on the WAAM, MIG, low carbon steel and the process that conclude in this research. WAAM is a popular metal 3D printing technology that have several advantages such as its high deposition rate, efficiency, and low price. It also has a ability to meet the manufacturing needs of medium to large (AI) components for automotive, aerospace and more others related industries. WAAM commonly used a laser-based system to commercial their 3D metal printing product but a bit expensive than used the traditional method that used efficient energy sources such as metal inert gas (MIG) and this was cheaper. The final product may get some defect and porosity such as a little hole will appear after welding when using MIG method.

##### 2.1.1 Additive Manufacturing (AM)

The developing intrigued in additive manufacturing (AM) technology in the last decade has been largely due to the advantages characteristics were points of this innovation in terms of making profoundly complex their geometrics in a relatively short time. As for now, most pertinent production and research exercises were focus on 3D printing using

powder bed technology (PBT), such as selective laser melting (SLM) and electron beam melting (EBM)(Ron et al., 2020).

The ability to produce sophisticated three-dimensional objects that are difficult or impossible to produce using standard manufacturing procedures has transformed the manufacturing paradigm in recent years, thanks in large part to additive manufacturing. Large metallic objects may be produced with the high deposition rates of wire and arc additive manufacturing (WAAM), which are much higher than powder-bed techniques, for example. Figure 2-1 show how robots are solving the biggest challenges in welding. Significant research initiatives are ongoing because of a growing interest in WAAM (Rodrigues et al., 2019).



**Figure 2-1 How robots are solving the biggest challenges in welding**

The most relevant engineering materials, the main deposition strategies adopted to minimise residual stresses, and the effect of post-processing heat treatments on improving mechanical properties of the part; this review paper aims to provide an overview of major

achievements in WAAM, highlighting process developments and variants for controlling microstructure, mechanical properties, and defect generation in as-built parts. When compared to traditional machining methods, additive manufacturing (AM) eliminates the need for additional resources like cutting tools, jigs, and coolant fluids altogether. To produce designed pieces and support structures, AM uses only the number of materials that are necessary to do so. As a result, less material would be wasted, and the impact on the environment would be lessened. In addition, AM allows for topological optimization, which saves resources. A wide range of industries rely on additive manufacturing (AM) technology to produce planned components as well as support structures if necessary. In this way, it is possible to limit the amount of garbage and the negative effects on the environment. In addition, AM allows for topological optimization, which saves resources (Le et al., 2020).

## 2.2 Wire Arc Manufacturing (WAAM)

The requirement for enhanced production efficiency of engineering structures is driving the development of wire arc additive manufacturing (WAAM), currently known as directed energy deposition-arc (DED-arc). Its ability to make preforms that are extremely close to net shape without the use of complex equipment, molds, or dies has the potential to reduce costs and lead times, enhance material efficiency, improve component performance, and reduce inventory and logistics expenses (Blindheim et al., 2019). WAAM is the oldest, ostensibly simplest, but least discussed of the additive manufacturing (AM) methods, having been developed in 1920 (Commonly known as 3D printing). The basic technique, which uses wire as a feedstock, has been used for decades to perform local repairs on damaged or worn components, as well as to build circular components and

pressure vessels. Figure 2-2 show the hidden complexities of Wire Arc Additive Manufacturing.

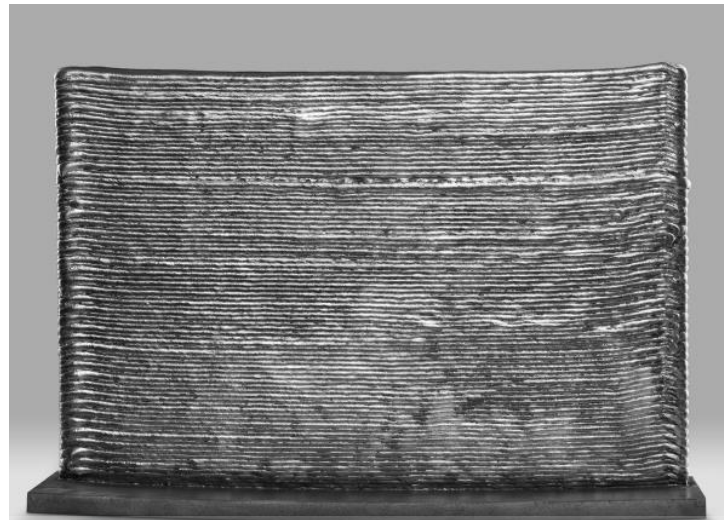


**Figure 2-2 The hidden complexities of Wire Arc Additive Manufacturing**

If you compare WAAM to PBT in terms of raw material and energy consumption, the WAAM process is about 80 percent more cost-effective in terms of raw material and energy consumption than the PBT method. While the standard PBT process can deposit 600 grammes of material per hour (g/h), WAAM can deposit roughly 10 kilograms per hour (kg/h). WAAM's open-air printing with a robotic arm and a localized protected area means that the printed product's dimensions are virtually limitless (Ron et al., 2019). Weld beads are layered on top of previously deposited layers in WAAM, which uses an arc welding flame as the energy source to create metal objects additively. Compared to powder-bed/feed AM systems, the deposition rates associated with WAAM are much greater (3–8 kg/h) since all the consumable wire is continually fed into the adopted electric arc or plasma and completely melted, leading to extraordinarily high deposition rates

connected with this process. Figures 2-3 show the diagram of WAAM process. Consequently, it is best suited for large-scale engineering components with simpler geometries and less complexity in their designs that can be produced using this method (Rafieazad et al., 2019).

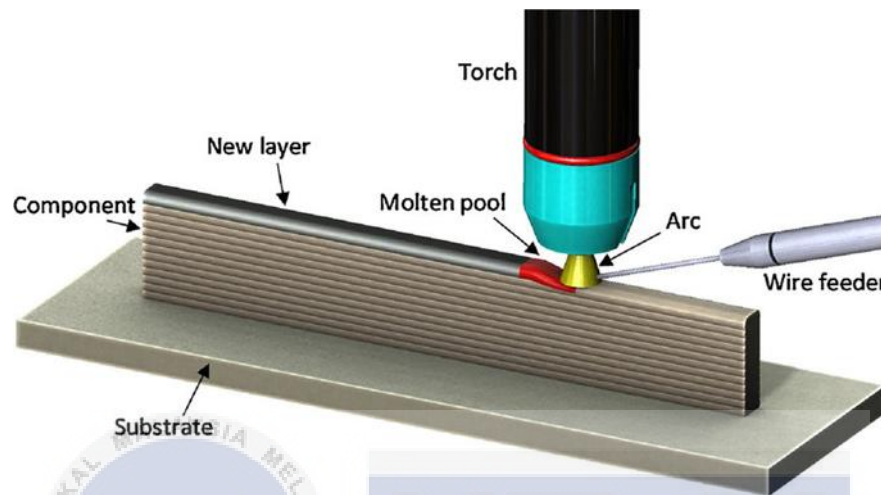


**Figure 2-3 Diagram of WAAM process**

### 2.3 MIG- Gas Metal Arc Welding (GMAW)

MIG welding is utilised in the automotive industry to repair automobile exhaust systems, as well as in the construction of homes and structures. Welding technology that is both more productive and better in terms of quality is being led by the GMAW process (Ibrahim et al., 2012). It is one of the most common welding techniques. This is a type of arc welding that employs the use of an electrode, which is a continuous wire. You'll also employ a shielding gas to prevent against contamination as it passes through the welding gun.

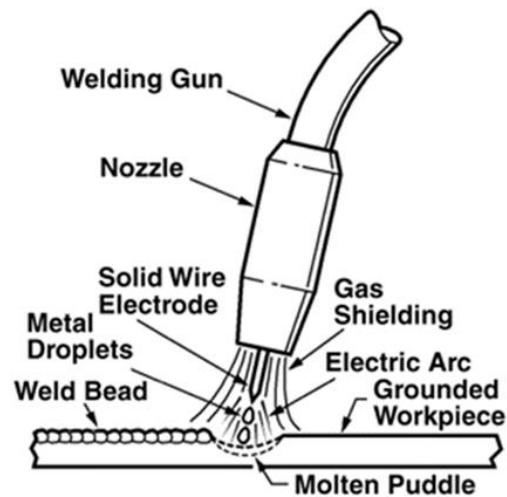


**Figure 2-4 Diagram of MIG process**

The assumption that "conventional" stable DC or sinusoidal AC current is utilised has been the basis for the standards relevant to arc welding manufacture. Naturally, weld quality metrics have been linked to various kinds of power output. It's been more than 30 years since commercially accessible sophisticated process waveforms were developed to manage process performance, but these were based on versions of early equipment designs, limiting their potential. Many existing fabrication standards use heat input or arc energy for the assessment of appropriate techniques and their continuing supervision, in addition to establishing electrical parameters required to control welding processes. Welding fabrication standards will need to be re-examined considering these new advancements, particularly the utilisation of more complicated transient waveforms (Norrish, 2017).

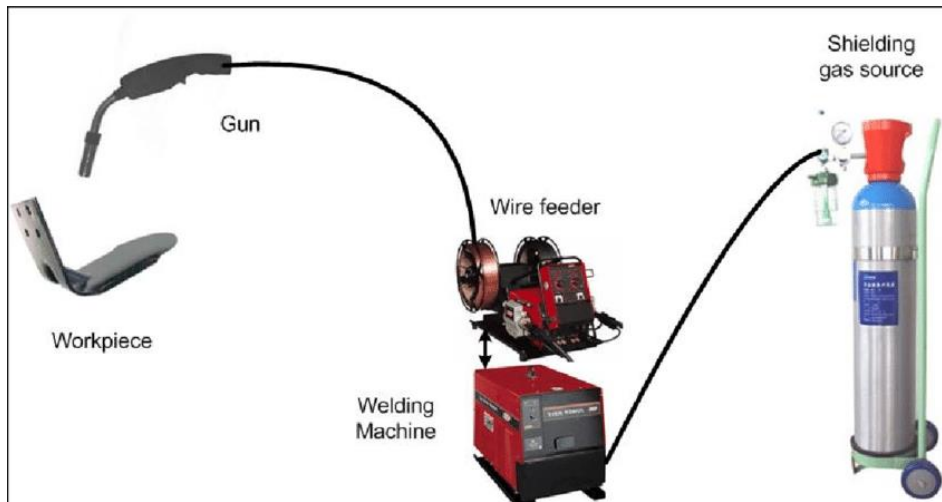


**Figure 2-5 Apparatus for MIG welding**

### 2.3.1 ABB WAAM Robots Welding

The ABB is a Wire Arc Additive Manufacturing (WAAM) robots that makes 3D printing metal parts process such as MIG, TIG or Plasma become simple and easily. This pre-engineered cell provides the user with the safety, flexibility, and performance needed to start designing new designs or manufacturing specific parts. This ABB robot achieves exceptional results by incorporating features such as ABB's superior path performance and absolute accuracy calibration, the robot's close motion coordination with an external axis, and seamless integration with the robot controller and Fronius welding equipment. It also has unrivalled RobotStudio and PowerPac capabilities (the Arcware PowerPac integrates flawlessly with the 3D Printing PowerPac). This robot has a built-in path for the robot arm as well as a positioner. Figure 2-6 above show the illustration of a robotic WAAM (Wire Arc Additive Manufacturing). Pre-engineered cells are less expensive and let the user to concentrate entirely on welding and fabricating parts without having to worry about equipment integration or safety (Arc, n.d.).

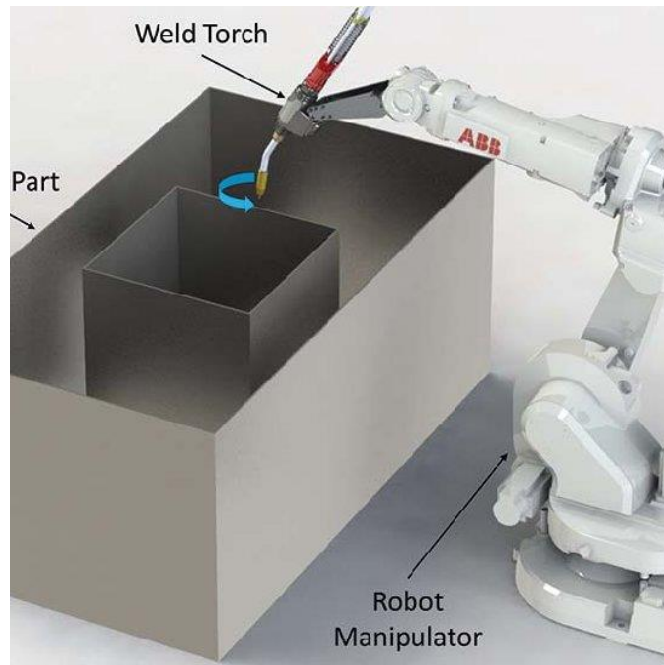


**Figure 2-6 Illustration of a robotic WAAM (Wire Arc Additive Manufacturing)**

The assumption that "conventional" stable DC or sinusoidal AC current is utilised has been the basis for the standards relevant to arc welding manufacture. Naturally, weld quality metrics have been linked to various kinds of power output. It's been more than 30 years since commercially accessible sophisticated process waveforms were developed to manage process performance, but these were based on versions of early equipment designs, limiting their potential. Many existing fabrication standards use heat input or arc energy for the assessment of appropriate techniques and their continuing supervision, in addition to establishing electrical parameters required to control welding processes. Welding fabrication standards will need to be re-examined in light of these new advancements, particularly the utilisation of more complicated transient waveforms (Yuan et al., 2020).

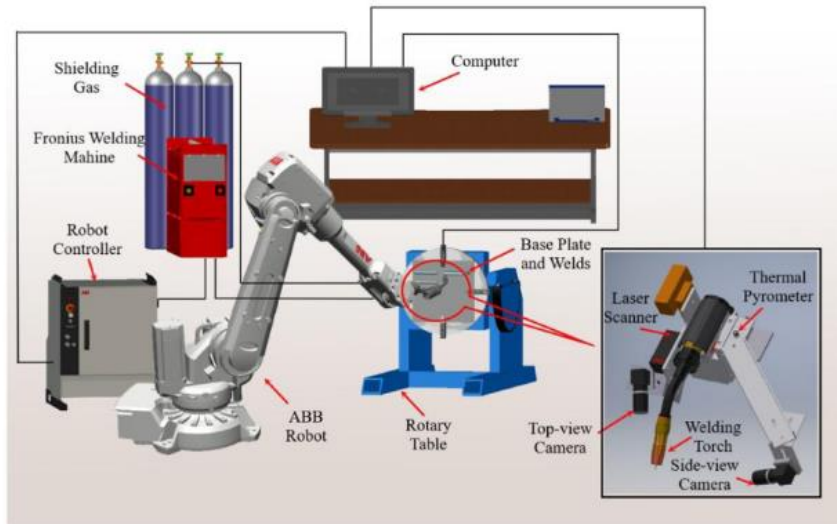


**Figure 2-7 Apparatus and Illustration process of welding**

### 2.3.2 Welding Current

When MIG welding, a higher current can cause spatter and damage to the work piece. Lower current settings in MIG welding cause filler wire to stick once again. With lower welding current, a larger heat-affected region is commonly evident because high temperatures must be used for longer periods of time to deposit the same quantity of filler materials. In fixed current mode, the voltage will fluctuate to maintain a constant arc current.

### 2.3.3 Low Carbon Steel/Mild Steel

Alumina Carbide based composites are routinely used in mechanical, automobile, ceramic and aerospace industries with numerous reinforcements. Reinforcements increase the physical, chemical, mechanical, thermal and tribological properties and make Al<sub>2</sub>O<sub>3</sub> suitable for a specific application. Alumina Carbide composites demonstrated high hardness, excellent chemical stability, superior coefficient of thermal expansion, enhanced thermal shock resistance and high abrasion resistance.

## 2.4 Filler Wire (ER308SL)

The WAAM approach was used to optimize those parameters, resulting in the desired geometry of single weld beads for producing 308L walls. The microstructure of WAAM 308L steel walls is characterized primarily by austenite dendrites developing vertically and residual ferrite present at grain boundaries of the austenite matrix. WAAM 308L walls have UTS, YS, and elongation values of 532- 553 MPa, 344-353 MPa, and 40-54%, which are comparable to those of wrought 308L stainless steel (UTS: 530-650 MPa, YS: 360-480 MPa, and elongation: 35-45%). As a result, the mechanical qualities of WAAM 308L steel walls are deemed sufficient for industrial applications. (Le et al., 2021)

	C	Si	Mn	Cr	Ni	Fe
ER70S-6	0.07	0.9	1.45	-	-	Rest
308LSi	0.01	0.7	1.9	20	9.5	Rest
St37	0.17	0.3	1.4	-	-	Rest

**Figure 2-8 Main chemical contents of feeding wires of 308SLi filler wire**

The 308LSi layer has a strong ferrite phase structure. Furthermore, peaks other than ferrite are observed at sites where the austenite phase is present. Because the compounds indicated in the preceding paragraph have similar diffraction degrees, the probability of the same chemicals being on the 308LSi side should be addressed as well. The mean hardness of the interface in the ER70S-6 layer at the transition to the 308LSi layer was found to be close to the hardness of the 308LSi layers. This could be attributable to less 308LSi dilution in the chemical composition during manufacture. It is believed that no development occurs in the microstructure of the 308LSi layer in the FGM section, which increases hardness at high rates, as occurs in the ER70S-6 layer.

### 2.4.1 Alumina Powder

Reinforcements based on alumina carbide are widely employed in mechanical, automotive, ceramic, and aerospace applications. Adding reinforcements to  $Al_2O_3$  improves the material's physical, chemical, mechanical, thermal, and tribological properties and makes it suitable for a certain use case. Alumina carbide composites had impressive mechanical properties, including high hardness, excellent chemical stability, superior coefficient of thermal expansion, better thermal shock resistance, and high abrasion resistance. Figure 2-9 show an alumina oxide powder.



**Figure 2-9 Alumina Oxide Powder**

The matrix and the reinforced particles in an Alumina Carbide composite form strong interface bonds due to the high degree of agglomeration between the two. As a result of the eutectic reaction, the graphite-based aluminium hybrid composite also displayed remarkable tribological behaviour. Table 1 shown the properties of raw material for Alumina Powder Carbide. (Nallusamy & S, 2021)

Properties	Alumina Powder Carbide
Chemical formula	Al <sub>2</sub> O <sub>3</sub>
Melting point	2072 °C
Density	3.986 g/cm <sup>3</sup>
Appearance	White
Particle size	90-100 nm
Form	Nano powder
Description	Trigonal

**Table 1 Properties of raw material**

#### 2.4.2 Titanium Carbide (TiC)

The effects of TiC content on the evolution of WAAM grain boundary structure, phase transition, grain distribution, interface misfit, and mechanical characteristics. The addition of TiC particles converted the columnar grains in the inner-layer zone into equiaxed grains, which eventually led to a decrease in the Al-free matrix's energy, so facilitating the growth of nuclei on the TiC substrate. Creating such components with great ductility and strength allows them to replace titanium alloys or stainless steel in rocket fuel tanks, missile seekers, and train bodies. Figure 2-10 show a picture of the titanium carbide. (Jin et al., 2021)



**Figure 2-10 Titanium Carbide**

### **2.4.3 Shielding Gasses for Welding**

To maintain the stability of the WAAM process, as is illustrated in Figure 2 -11, there are many factors in WAAM that must remain constant. The most frequent shielding gases employed in the welding process are carbon dioxide, argon, helium, and oxygen; nevertheless, each of these gases has a unique effect on the performance of the welding process due to the features that are unique to it. Welding is one of the most common applications for carbon dioxide (CO<sub>2</sub>) gas, which is also the least expensive reactive gas. The welding parameters such as current, voltage, and wire feed speed are the most important variables to consider while working with welding technology. In addition, the process of welding can be a short circuit, an impulse, or a particular digitally controlled process. Another factor to consider is whether there is a shielding gas present, in addition to the additive (or filler) substance. The influence of the shielding gas that was utilised for WAAM on the geometric quality of the piece that was welded is the primary focus of this investigation (Liew et al., 2019).

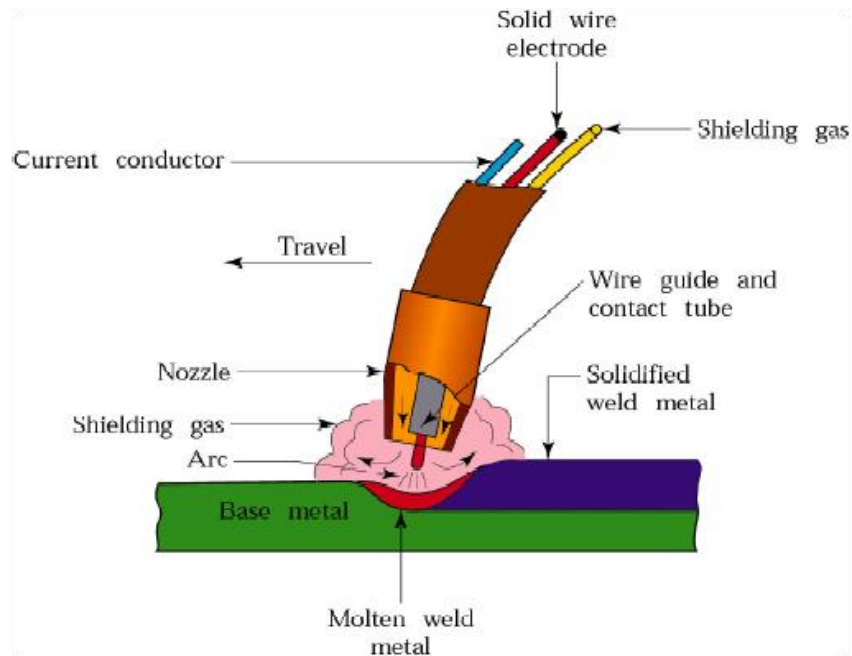


**Figure 2-11 Illustration on how shielding gasses work**

Md. Ibrahim Khan explained that the process by which two or more components are welded together to form a single whole is referred to as welding. There are several different processes for welding, including Gas Metal Arc Welding (GMAW), Gas Tungsten Arc Welding (GTAW), Manual Metal Arc Welding (MMAW), and others. In this investigation, the Gas Metal Arc Welding technique is utilised, and the welding procedure makes use of not one but two distinct gases, namely carbon dioxide (CO<sub>2</sub>) and argon (Ar). The choice of shielding gas during the Gas Metal Arc Welding (GMAW) process has a significant impact on both the quality and the strength of the welded joint that is produced. The molten weld puddle and the electrode need to be shielded from the oxygen, nitrogen, and moisture that are present in the air. This is the basic purpose of all shielding gases. A temporary protective pocket of gas is formed over the weld puddle and around the arc as shielding gases flow through the welding gun and exit the nozzle surrounding the electrode.

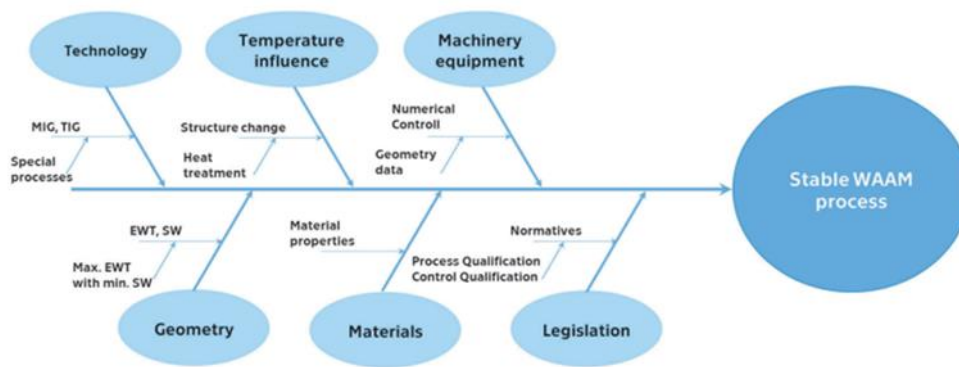


**Figure 2-12 Flow chart of stable WAAM process**

This pushes the air out of the way and forms the pocket around the arc. Because the shielding gas plays such a vital role in the welding process, any modification to the gas mix or flow parameter will influence the arc transfer characteristics and the quality of the weld that is produced. Figure 2-12 show the flow chart of stable WAAM process. Under the intense heat of the arc, carbon dioxide and argon react in distinctively different ways. Argon is an inert gas, meaning it does not react with any other chemicals or elements. It is also approximately 1.4 times heavier than air, making it unsuitable for use in sustainable environments. Table 1 show the parameter of shielding gasses. Argon does not contribute any chemicals to the molten pool during the GMAW process; rather, it acts as a barrier between the pool and any contaminants that may be present (Khalid et al., 2017).

**Table 2 Parameter of Shielding Gasses**

Gas	Molecular Weight (gm/mol)	Specific Gravity	Density		Ionization Potential	
			$10^{-9}$ kg/cm <sup>3</sup>	g/litre	$10^{-18}$ J	eV
Argon(AR)	39.95	1.39	3.93	1.784	2.52	15.7
Carbon Dioxide(CO <sub>2</sub> )	44.01	1.53	4.36	1.978	2.26	14.4
Helium(He)	4.01	0.1368	0.39	0.178	3.92	24.5
Hydrogen(H <sub>2</sub> )	2.016	0.0695	0.19	0.090	2.16	13.5
Nitrogen(N <sub>2</sub> )	28.01	0.967	27.6	12.5	2.32	14.5
Oxygen(O <sub>2</sub> )	32.00	1.105	3.15	1.43	2.11	13.2

## 2.5 Optimization of Microstructure Process

Microstructures is a compositional/structural inhomogeneities that might include spatially scattered phases of various compositions/structures, grains of various orientations, and structural flaws. Microstructure also known as a material structure that only can see at the micro level. They are structures revealed by a microscope at magnifications greater than 25 times on an item, creature, or substance. To investigate and identify the characteristics of materials, this microstructure method is a best way to read and make an analysis for the surface and structure of the material that have been created at the end of the process.

### 2.5.1 Analysis Effect of Heat Input in WAAM Process

The topic in this section is on the three primary effects of heat input, which are the macrostructure, the microstructure, and the mechanical properties of the material. The influence of heat input, which is discussed in this part, as well as a summary of such discussion, can be found at the conclusion of each theme classification. A few studies on wire arc additive manufacturing of stainless steels have recently been published, focusing on the chemical composition of the filler metals, process parameters, process modelling, flaws, residual stress and distortion, microstructure, and mechanical properties.

### 2.5.2 Pyrometer

Directed Energy Deposition (DED) encompasses Additive Manufacturing (AM) technologies in which concentrated heat energy is employed to melt materials as they are deposited. Wire+Arc Additive Manufacturing (WAAM) is a DED technique that utilises an electric arc as its thermal energy source and metallic wire as its material. Using potential solutions for emissivity determination and mitigation of interferences from arc/pool

radiations, it is demonstrated that IR pyrometry is a viable technique for non-contact interpass temperature measurement with high spatial resolution (small spot size) and promising control implementation potentials. Figure 2-13 show a pyrometer that can read a temperature. [pyro1.pdf](#)



**Figure 2-13 Pyrometer**

Heat accumulation is a crucial element that affects the stability of the WAAM process in terms of geometrical precision, deposition errors, microstructural evolution, and as-fabricated part material properties. Ma et al. conducted an experiment in which a basic Ti-Al component was manufactured utilising GT-WAAM. When the interpass temperature changes from 100°C to 500°C, the alpha phase fraction in the microstructure reduces by approximately twofold, resulting in a decrease in hardness values. Denlinger observed in a separate investigation that the distortion and residual stresses of as-fabricated titanium and nickel alloy components were considerably influenced by the interlayer dwell time, which is directly related to the thermal properties. (Wu et al., 2017)

## **2.6 Microstructure Characteristics of Samples**

WAAM stainless steel microstructures are mostly determined by the heat history of the processes. The thermal cycle, which includes repeated heating and cooling, develops non-equilibrium microstructures in the deposited pieces during WAAM processing. The

microstructure of the printed (WAAM) alloy ER70S-6 at both the transverse and the longitudinal cross-sections. Following an arc welding procedure, this resulted in a typical microstructure of low carbon steel with a reduced amount of secondary pearlite phase, as seen in the preceding sentence (Ron et al., 2019). The intrinsic quick solidification features of the WAAM method, in addition to the slight changes in carbon content, are primarily responsible for the relatively lower amount of pearlite phase that was found in the printed alloy. A trace quantity of residual austenite was found embedded in the ferrite matrix of both alloys, which was to be expected.

Figure 2-14 presents the overall microstructure of the ER70S-6 steel wall at various places, illustrating the variation in the microstructure as one moves from an area in the vicinity of a fusion line towards the centre of the melt pool (top left corner of the image). The dominant microstructure of each melt-pool centre is depicted in Figure 2-13 b and d. This microstructure is composed of the typical fine polygonal ferrite (F) as the primary phase and a low-volume fraction of the lamellar pearlite (P) phase, which has primarily formed along the ferrite grain boundaries. Both phases can be seen in the figure. A WAAM-fabricated ER70S-6 wall was examined in a prior work, and similar microstructural findings were reported for that wall. In addition, the production of acicular ferrite together with bainite areas (AF + B) near to the melt-pool barrier was verified by taking a closer look at the microstructure along the melt-pool boundaries (Fig. 2-13, e). This transition in microstructure is brought on by the overlapping scanning lines and the solidification of individual melt pools, both of which result in different thermal histories from the centre of each melt pool to the boundaries of its adjacent melt pools. Therefore, this transition in microstructure can be seen in the final product. As a result of the fact that the fusion borders go through a more rapid cooling process during the solidification

process than the centre of the melt pools does, the production of some non-equilibrium AF + B phases was observed in the region next to the fusion lines (Rafieazad et al., 2019).

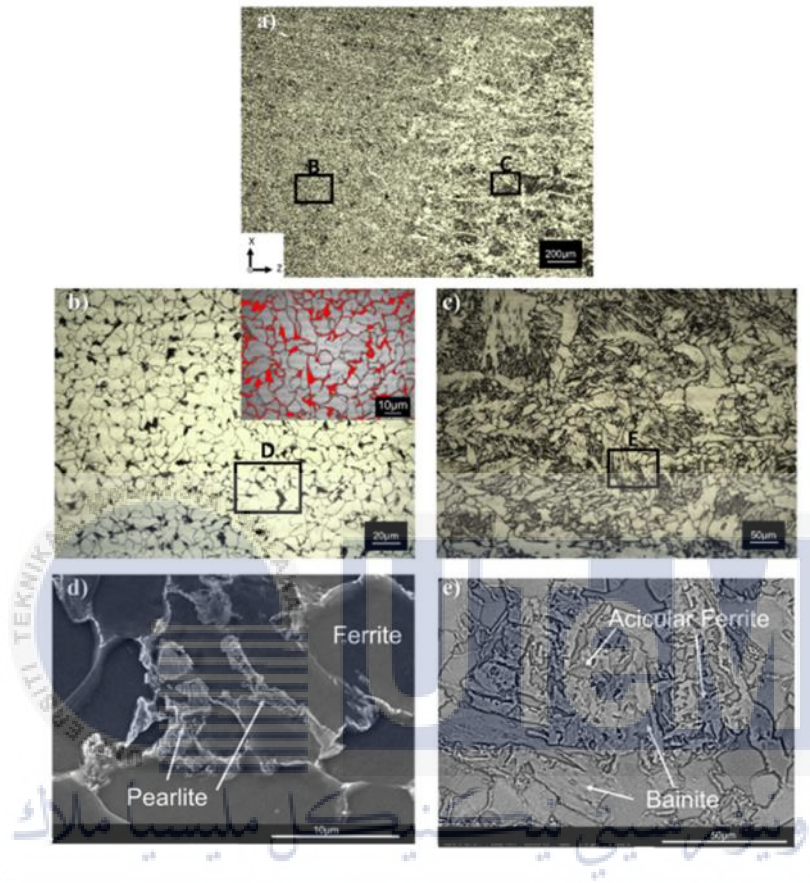


**Figure 2-14 Optical micrographs taken from the WAAM-ER70S-6 steel wall at the fusion line and center of the melt pool. b Higher magnification of the enclosed area in a shown by B, and the inserted image shows an example of a phase fraction analysis micrograph**

For the purpose metallographic examination, samples were cut with a metallic saw in the following manners: transversely cross sectioned (XZ), longitudinally cross sectioned (YZ), and sectioned between layers (XY) (axes referenced in Fig 2-14). Subsequently, the samples were mechanically polished and etched with a 2 percent Nital solution (Nitric and Ethanol acid). After the samples had been prepared for metallographic analysis, both the microstructures and the macrostructures were viewed using a microscope by the brand

name Eclipse MA200 (Nikon). To conduct a macro-examination and Vickers hardness test, samples were taken in a transversal direction from the centre of the walls at three different heights: the top, the middle, and the bottom. Testing for Vickers hardness was carried out at room temperature using a machine known as the Duramin A-300 (Struers), in accordance with the standard ISO 6507-1 (Bilbao & Lamikiz, 2020).

To test the tensile strength of the overlapped and oscillated walls, twelve tensile specimens with precise dimensions (neck diameter 4 mm and length 22 mm) were cut from the walls. In the tensile tests, some of the specimens were cut in a vertical orientation, while others were cut in a horizontal orientation. In accordance with ISO 6892-1, specimens of tensile force were manufactured. An Instron 5585H electronic equipment was used to conduct the uni-axial tensile test while the temperature was kept at room temperature. A contact extensometer Instron EX2620-602 with a load cell of 100 kN was utilised during the tensile testing that was carried out. In this instance, as the primary goal is to produce walls that adhere as precisely as possible to the specified geometry (wall width 20 mm and wall height 70 mm), the control volume in both walls encompasses all the deposited material in an area that is 20 mm wide (x) and 20 mm long (y). Since the laser scans every two layers in succession, the control volume height (z) is provided every two layers in succession.

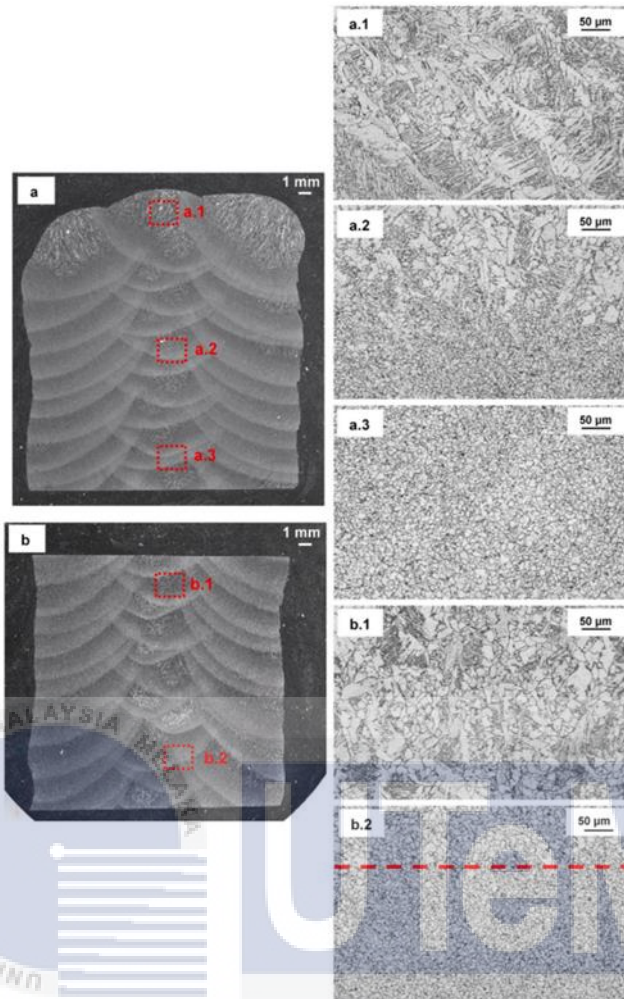


**Figure 2-15** (on the left) are macrostructures of the top and bottom halves of the overlapping wall in the transversal direction (the plane XZ), and (on the right) are microstructures of the overlapped wall.

## 2.7 Microhardness Properties

For the purpose micro-hardness measurement, the samples were cut in half perpendicular to the direction of laying and then processed using standard metallographic procedures. The measurement was taken at a load of five hundred grammes at an incremental spacing of twenty-five millimeters. NiTi LAM has a micro-hardness value of 370 VHN, while NiTi MBAM has a micro-hardness value of 415 VHN, and CuAlNi has a micro-hardness value of 324 VHN. It can be observed quite plainly that the micro-hardness

value of NiTi MBAM has grown since it was last measured. Despite fact that the surface of the NiTi LAM samples had some dents in them, their microhardness was significantly lower than that of the NiTi MBAM samples. There is a correlation between the rise in microhardness and the faster cooling rate of NiTi MBAM, so this must be the cause. The decrease in the microhardness of the CuAlNi sample must be attributed to the presence of copper and aluminum, given these elements are present. The sample underwent a heat treatment that was uniform throughout, and this is another factor that may have contributed to the reduction in microhardness. Figure 2-16 show a fMicrohardness graph of a NiTi LAM b NiTi MBSM c CuA1Ni.

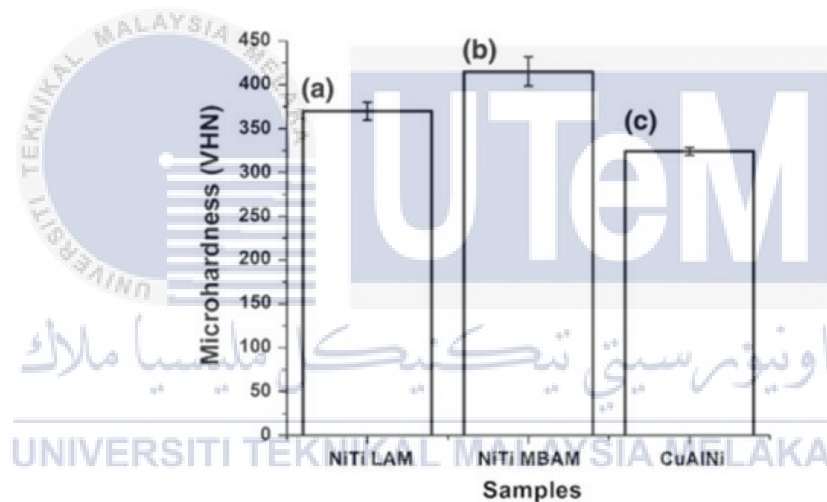


**Figure 2-16 Microhardness graph of a NiTi LAM b NiTi MBSM c CuA1Ni**

It was discovered that each of the manufactured samples reveals the exact same progression in hardness, as depicted in Figure. The average value of the samples' upper section displays the highest level of hardness, whilst the average value of the samples' middle region reveals the lowest level of hardness. This observation agrees with the microstructures that was found. According to this relationship, the harnessing of materials achieves a higher level when the grain size in the microstructure is smaller.

The microhardness of the upper section is significantly greater than that of the other parts because of the presence of Widmanstatten structures (see Figure 2-17). The microhardness values of the lower region are significantly greater than those of the middle region. This is because the lower region contains lamellar structures, as seen in Figure 2.18c. In addition to this, the sample that was created with a lower heat input exhibits considerably better microhardness in each zone. This is the case regardless of the region. The reason for this is that a larger heat input results in a coarser grain size in the microstructure of the material that is being formed. Figure 2-18 show a Microstructure of built materials in the upper region (a), in the middle region with lower magnification (b), the lower region (c)The microhardness of the samples S1, S2, S3, and S4 ranged from 162 minus 2.88 to 192 minus 4.30, 162 minus 3.51 to 191 minus 3.96, 160 minus 2.30 to 182 minus 2.30, and 157 minus 3.11 to 179 minus 3.16 (HV5), respectively(Le et al., 2020).

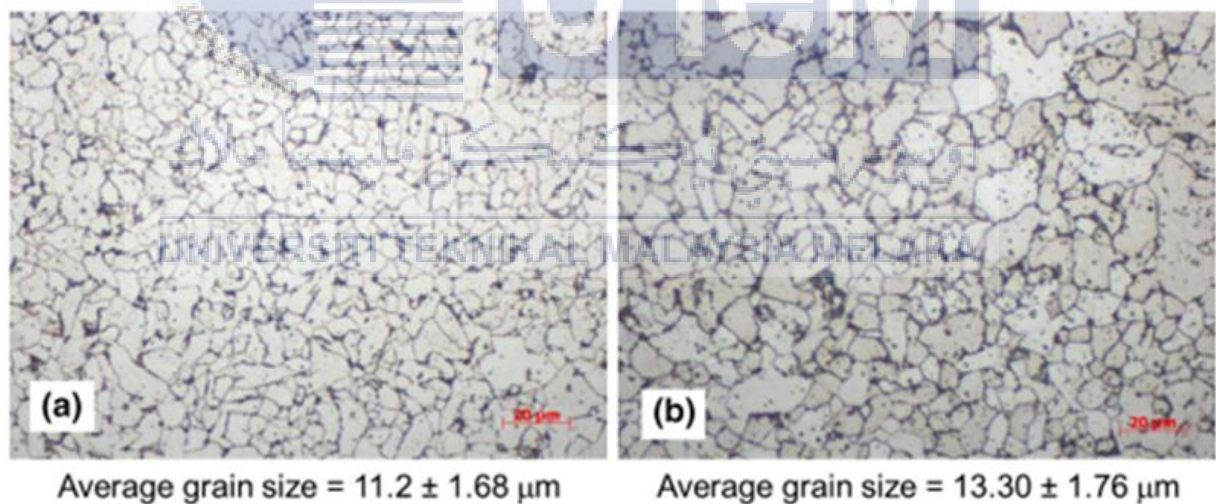


**Figure 2-17 Microhardness samples**

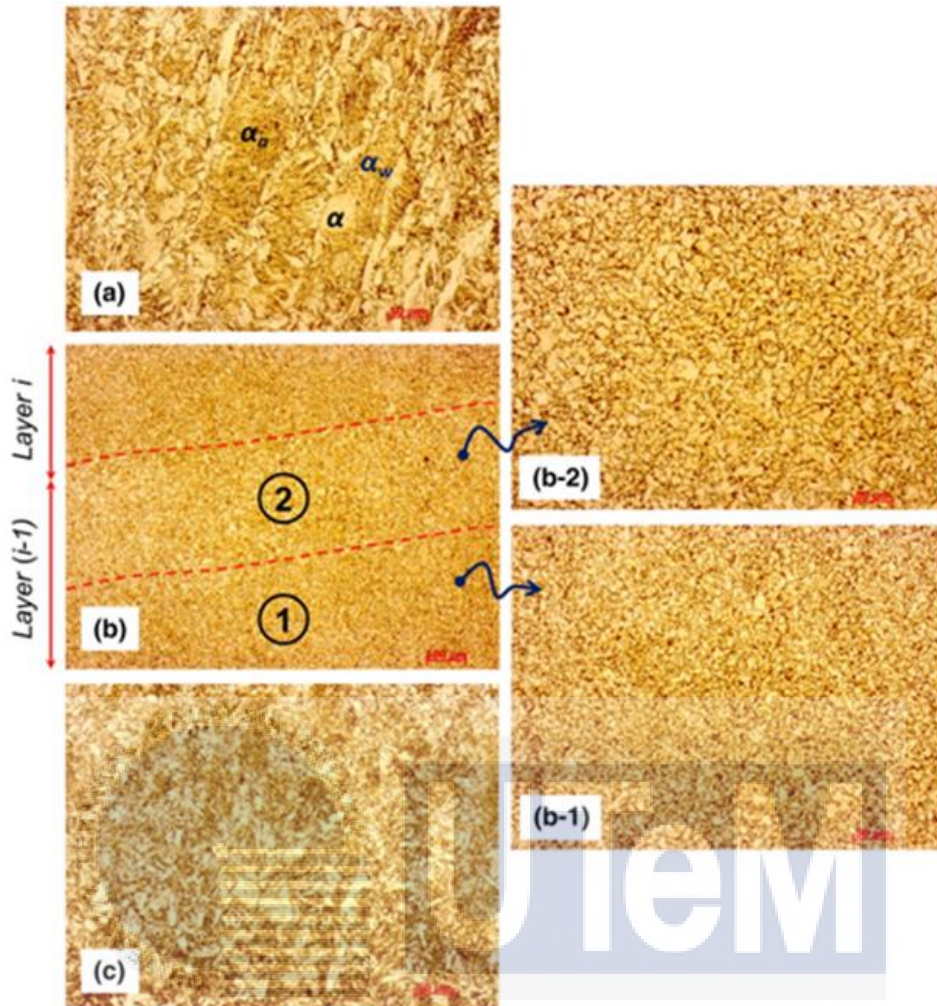


Figure 2-18 Microstructure of built materials in the upper region (a), in the middle region with lower magnification (b), the lower region (c)

## CHAPTER 3

### METHODOLOGY

#### 3.1 Introduction

In this chapter, we will be discussing the research method study that was done for this project. It comprises a theoretical analysis of a branch of knowledge's corpus of procedures and principles, with methodologies from different fields differing based on how they've developed over the course of their respective histories. The investigation of the process properties link between different types of materials is the purpose of this study. The parameter is one of the most important factors that affects the properties. To determine the optimal parameters for carrying out this welding operation, some research was compiled from a variety of articles. The execution of this experiment involves a lot of different steps. To begin, the material that will be utilized in the project is chosen after it has been evaluated to determine whether it satisfies the requirements given in the specification. After the experiment has been set up, the parameter for the welding will be decided, and then the experiment will be carried out.

#### 3.2 Flow Chart Research

This thesis presents a new and integrated analytical approach to estimate TL of MV distribution network. The essence of the approach used in this project is centered on the concept of EFM and RF. The selected approach is based on quantitative type, which aims to develop analytical model to calculate and analyze the TL on MV distribution network component (i.e. MV feeders and transformers). The method (design) is experimental,

which utilizes empirical modelling and statistical approach. Subsequently, Figure 3.1 shows the research design of this thesis.

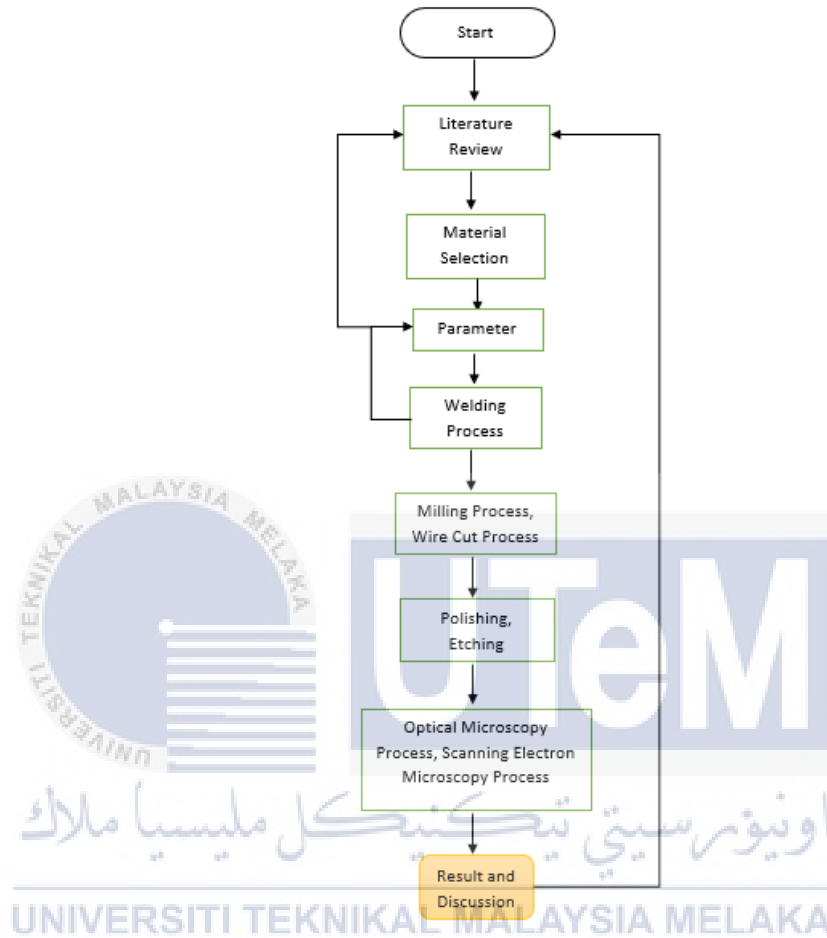


**Figure 3-1 Flow Chart methodology of the Microstructure Experiment Process**

Gantt charts are helpful for project planning and scheduling. They aid in estimating the duration of a project, identifying the required resources, and organising the sequence in which tasks will be completed. Additionally, they are useful for managing task dependencies. Gantt charts facilitate the organisation of projects, enhance project visibility, and keep everyone on track. Additionally, Gantt charts assist managers in allocating resources when and where they are required. And they foster teamwork among project team members.

### 3.3 Material Selection

In the process of designing any physical thing, material selection is necessary. The primary objective of material selection in product design is to keep costs as low as possible while yet achieving the desired levels of performance. Candidate materials' qualities and costs are the first considerations in a systematic selection process. The use of a material index or performance index relevant to the required attributes of the material is often beneficial in the selection process of materials.

To quantify microstructural traits, it is necessary to characterise both morphological and material properties. Image processing is a reliable method for identifying morphological characteristics such as volume percentage, inclusion morphology, void, and crystal orientations. In order to acquire micrographs, optical and electron microscopy are frequently employed. Nanoindentation is a rigorous technique for determining material properties at the micron and submicron level, for which standard testing is impractical. Conventional mechanical testing, such as tensile testing or dynamic mechanical analysis (DMA), cannot provide any indication of the microstructural characteristics of a material. Nevertheless, nanoindentation can be utilised to determine the local microstructural characteristics of both homogeneous and heterogeneous materials. Microstructures can also be defined using high-order statistical models that extract from the images a complex set of statistical attributes. Then, these traits can be utilised to generate a variety of other stochastic models.

For this research and project, There are five types of materials from which we select and make use. The initial ones were constructed out of ER308L Si arc wire.

Following that was a plate made of low carbon steel, which was going to be used as the welding base. We decided to utilise shielding gases since there is a possibility that they will protect the weld area from oxygen and water vapour. Alumina oxide powder and Titanium Carbait were mix with ER308L Si and have been carried out to know the hardness and types of microstructures. The welding procedure has been carried out with the assistance of ABB WAAM Robots Welding. If we use these robots, the procedure will become much simpler, and all we will need to do to get it started will be to give the robots their instructions.

### 3.3.1 ER308L Si Arc Wire

Similar to 308, but with less carbon, is 308L stainless steel. Stainless steel grade 304 submerged arc welding is a common application. Under non-corrosive conditions, it can also be utilised to weld stabilised grades 321 and 347. So we used this type of wire in this experiment. The investigated WAAM process adopts 308LSi stainless steel as swire feedstock, therefore resulting in 3D-printed welded stainless steel elements.



**Figure 3-2 ER308L Si Arc Wire**

Furthermore, it is less likely that intergranular carbide precipitation will occur in ER308L than in ER308 due to its reduced carbon concentration. This results in increased resistance to intergranular corrosion without the need for traditional stabilisers like niobium or titanium. Figure 3-3 show the stainless steel ER308L Si that have been used in this research. ER308L wire is designed for use in applications such as welding and overlay of similar composition base metals such as 304L. Uses for 308L. that require exceptional atmospheric corrosion resistance include those in the chemical and petrochemical sectors, distilleries, dairies, and restaurant equipment.

### 3.3.2 Shielding Gasses (Argon + Co2 Gas)

Shielding gases are inert or semi-inert gases that are often used in welding, especially in gas metal arc welding and gas tungsten arc welding, which are more commonly known as MIG (Metal Inert Gas) and TIG (Tungsten Inert Gas), respectively. Their job is to keep oxygen and water vapour from getting into the weld area. Depending on what is being welded, these gases in the air can lower the quality of the weld or make it harder to weld. Other arc welding methods also use different ways to keep the atmosphere away from the weld.



### Figure 3-3 Shielding Gasses (Argon+Co2)

The molten weld pool should not be allowed to come into contact with the oxygen, nitrogen, and hydrogen that are present in the air atmosphere. This is the primary goal of the shielding gas. The interaction of these components with the weld pool can lead to a number of complications, such as porosity (holes inside the weld bead) and an excessive amount of spatter. A poor selection of a welding gas can result in a porous and weak weld, or it can lead to excessive spatter. While the latter does not impair the weld itself, it does result in a loss of productivity due to the effort required to remove the scattered drops of weld spatter. Figure 3-4 show the shielding gasses that has been used in this experiment and Table 3 show the clasification of shielding gasses for arc welding.

**Table 3 Clasification of shielding gasses for arc welding**

Designation		Volume Percent (Vol %)						Common Application	Notes
Group	Code	Oxidising		Inert		Reduced	Slow-responding		
		CO <sub>2</sub>	O <sub>2</sub>	Ar	He	H <sub>2</sub>	N <sub>2</sub>		
R	1			Rest <sup>2</sup>		>0 to 15		TIG, plasma welding, plasma cutting, backing	
	2			Rest <sup>2</sup>		>15 to 35			
I	1			100				MIG, TIG, plasma welding, backing	
	2				100				
	3			Rest <sup>2</sup>	>0 to 95				

### 3.3.3 Mild Steel

Mild steel is a form of carbon steel that has a lower percentage of carbon than other types of carbon steel. Mild steel, which also goes by the name low carbon steel, has an amount of carbon in its composition that ranges somewhere between 0.05 and 0.25 percent

by weight. In contrast to this, high carbon steel, which can contain as much as 2.5 percent carbon by weight, can have up to a composition of. Mild steel is not considered to be an alloy steel because it does not include significant quantities of any elements other than iron and ferrite.



**Figure 3-4 Low carbon mild steel plate**

Mild steel is one of the varieties of steel that is used the most frequently because it is suitable for the production of goods in a wide range of different business sectors. There are a wide variety of applications for mild steel, including structural steel, autos, furniture, fencing, and far more. How strong is mild steel? Because it includes a lower proportion of the alloy that causes hardening carbon than other types of carbon steel, mild steel is an example of a material that is considered to be relatively ductile. It only has a tensile strength of about 400 MPa, which is not very high. Figure 3-5 show low carbon mild steel plate that been use in this project.

### 3.3.4 Alumina powder

The chemical formula for alumina powder is  $Al_2O_3$ , making it a type of ceramic. These powders are distinguished by their structure, purity, hardness, and specific surface area. Although there may appear to be only subtle variances between the items, the physicochemical features of the two ranges are very distinct from one another. We build a paste out of the alumina powder, but before we do so, we combine it with a little bit of methanol and some water. After that, we combine it with arc wire made of stainless steel before abb robot start welding.

### 3.3.5 Titanium Carbide (TiC)

TiC, or titanium carbide, is a refractory ceramic substance with a hardness close to that of tungsten carbide (Mohs 9-9.5). NaCl (face-centered cubic) crystals have the appearance of black powder. It's found in nature as a variety of the extremely rare mineral khamrabaevite (in Russia). Typically, the size of its crystals in nature is between 0.1 and 0.3mm. Titanium carbide has a shear modulus of 188 GPa and an elastic modulus of around 400 GPa. We build a paste out of the TiC, but before we do so, we combine it with a little bit of methanol and some water. After that, we combine it with arc wire made of stainless steel before abb robot start welding. Figure 3-6 show the compound of Titanium Carbide Powder.



**Figure 3-5 The Compound of Titanium Carbide Powder**

### **3.3.6 Kalling' No. 2**

Kalling's No. 2 etching acid have a highly acid that can make microstructure formation in high-chromium steels (more than 5% chromium) by an etching reagent. 5 g of copper chloride, 100 mL of hydrochloric acid, 100 mL of alcohol, and 100 mL of water make up the solution. Surely this Kalling's acid usually used for stainless steel materials. So, we decided to utilize it to this experiment after we study from lots of journal and articles. Figure 3-7 are the high acidic kalling's no.2 that have been used for etching process.

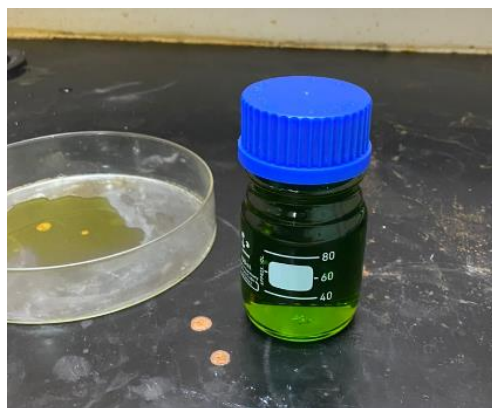


**Figure 3-6 The High Acidic Kalling's No.2**

### 3.4 Parameter

The goal of this study is to deposit between 30 and 50 total weld layers by experimenting with a wide range of values for both the travel speed and the wire feed speed. The length of 270 millimeters has been utilized as the measurement standard. After running a few simulations with various sorts of parameters that we collected from sources like journals and articles, we arrived at the conclusion that these parameters in Table 4 should be used. The values for voltage, wire feed speed, travel speed, and current are all included in this table. We did some calculations, and if we take this parameter, we will end up with a width of between 8 and 9 millimeters, which we believe will make it simpler to continue the tensile test. Despite the fact that we altered the WFS in addition to the travel speed, there were still other components of the operation that remained unchanged.

**Table 4 Parameter of robot welding ABB**

Voltage	Wire Feed Speed (WFS) (m/s)	Current (A)	Travel Speed (mm/s)
19	8	138	200

The basic experiments were planned and carried out by determining the values of the travel speed and WFS to obtain a variety of heat inputs at various levels. This allowed for the acquisition of data that was useful for analyzing the results of the tests. This was done to construct the test samples. At the outset, it was determined that there was a SOD that was equal to five millimeters between the welding flame and the substrate. Following the application of the first layer, the increment of each succeeding layer was kept at a constant 2.0 millimeters throughout the process.

### 3.5 Run Experiment

The configuration of the WAAM walls as well as the fabrication method is depicted in Figure. For the purposes of this investigation, the rolled structural low carbon steel base plate with the dimensions (300 x 200 x 12 mm<sup>3</sup>) was chosen as the material of choice. The deposition of WAAM walls began at the midpoint of the width of the foundation plates, and an oscillation pattern was used to deposit each layer on top of the previous one in order to achieve a wall with a sufficient thickness of about 50 millimetres. In prior research, it was discovered that the oscillation pattern allows more accurate control of wall thickness compared to the parallel deposition technique. This was proven to be the case when comparing the two strategies. In addition, because it is a more heat-intensive procedure, there is a lower chance of fusion flaws occurring. Building a single layer also requires less time than the alternative method, which involves depositing many straight wiring lines next to each other, shutting the arc off, and moving the torch to a different position.



**Figure 3-7 Setup for fabrication process**

### **3.6 Result Recorded**

A wire-cutting machine and milling machine must be used to remove the newly welded material. The material will be separated into more pieces and can be divided into tensile test and hardness test impact before the microstructure procedure can be done.

#### **3.6.1 Surface Grinding**

Surface grinding is a finishing procedure that uses a rotating abrasive wheel to smooth the flat surface of metallic or nonmetallic materials, giving them a more polished appearance by removing the oxide layer and contaminants from the work piece surfaces. But in this project, we used this process to remove rough and uneven surface to facilitate locking by machine milling before the milling process is carried out. This will also achieve a functionally desirable surface. We used a hand grinder to remove uneven and even surfaces in the surface grinding process.

#### **3.6.2 Milling Process**

The removal of material from a workpiece is accomplished through the machining process known as milling, which makes use of rotary cutters to perform the cutting action. This can be accomplished by altering the direction on one or more axes, as well as the speed and pressure of the cutter head. In addition to being able to grind and turn materials, milling machines are known as multitasking machines (MTMs). The cutter fitted on the milling machine helps remove material from the work piece's surface. The material is removed from the milling machine once it has cooled. In this experiment FM-16VS model made in Taiwan and date of manufacturing in 2012. Figure 3-9 shown the Milling Machine.



**Figure 3-8 Milling Process**

A milling cutter is a cutting tool with sharp teeth that is attached to a milling machine and rotates quickly. This milling device utilizes use of face mill points due to the relative hardness of the material being worked. We went with face mill points since they're hard to damage while still doing their job of cutting and smoothing. By feeding the workpiece into the rotating milling cutter, small chips of material are cut from the workpiece to make the shape you want. Milling is usually used to make parts that are not axially symmetrical and have many features like holes, slots, pockets, and even three-dimensional surface contours. Parts that are made entirely by milling often have custom fasteners or brackets that are used in small quantities or for prototyping.

### 3.6.3 Wire Cut Process

Wire-cut EDM is frequently utilized for cutting plates with a thickness of up to 300 millimeters, as well as for the manufacturing of punches, tools, and dies out of hard metals that are difficult to produce using conventional methods. The wire is maintained in its position by upper and lower diamond guides, and the complete assembly is centered within a water nozzle head. The wire is never stopped being unwound from the spool. The wire-cutting process makes use of water as its dielectric fluid, managing its resistivity as well as its other electrical properties with filters and PID-controlled de-ionizer units. The debris that has been cut is carried away from the cutting zone by the water. Figure 3-10 shown the wire cut process and the results of wire cut process.



**Figure 3-9 On the left side, there is a picture of the wire cut process with an EDM wire-cut machine. On the right, there is a picture of a dog bone that has been cut to the right size for the next step.**

### 3.6.4 Mounting Specimen process

In most cases, mounting comes in as the second step of the process, following sectioning. The material that was sampled is encased in a plastic shell during the mounting process, which also serves to prepare the sample for the subsequent metallographic grinding and polishing step. Mounting makes polishing using a metallographic polishing equipment easier to grasp and stable. In order to make a perfect mounting of this specimen,

we use a metallography press mounting machine. Figure 3-11 shows the Phenolic Powder (Black) Mounting Compound Cat. No.CM-2001B-5KG that is used to make the mounting compound. This makes it easier to polish.

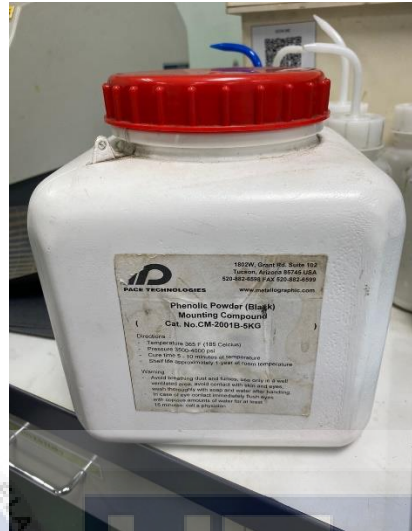
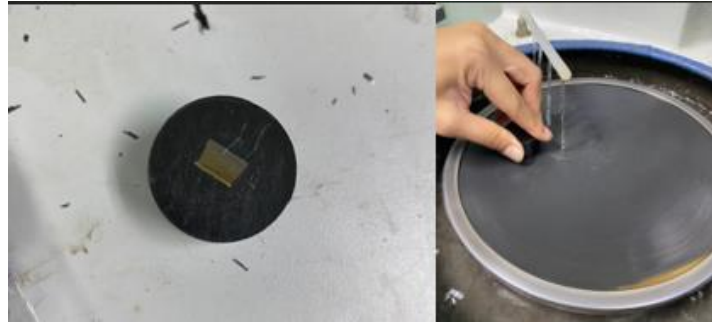


Figure 3-10 show a Phenolic Powder (Black) Mounting Compound

### 3.6.5 Polishing Process

Polishing is the process of creating a smooth and shiny surface by rubbing or applying a chemical treatment, leaving a surface that is clean and has a substantial specular reflection. To begin, sand the surface until it is smooth, lustrous, and free of scratches. The next step is used a chemical liquid and a polishing cloth to make the specimen's surface bright and reflective.

Figure 3-12 shows the prepared mounting compound that will make the polishing process easier. We use sandpaper with grits from 80 to 3000 to make sure the surface of the specimen is smooth and free of scratches. We then use a polishing cloth to make the surface of the specimen smooth and shiny before the etching process.



**Figure 3-11** show a condition of specimen after mounting at the left side. At the right side show a picture of polishing process using a sandpaper.

### 3.6.6 Etching Process

Etching is the process of creating an intaglio (incised) design in metal by cutting into the unprotected regions of the metal surface with a strong acid or mordant. Many other chemicals and materials could be employed in a modern production setup like this one. Along with engraving, it is the most essential printmaking technique for works by past masters. Before etching can begin, the plate must be polished so that any blemishes or scratches on the surface are gone. The ground is the uniform coating of acid-resistant varnish or wax applied once the surface is perfectly smooth.

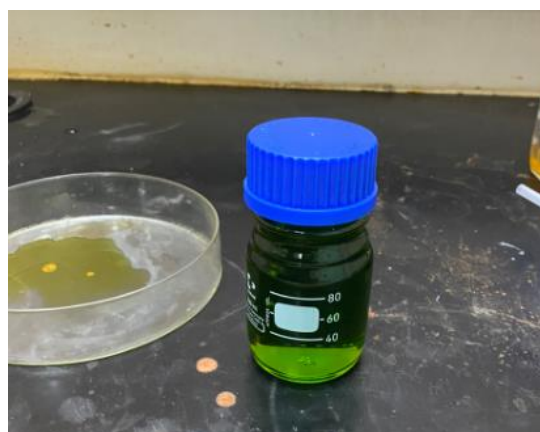


**Figure 3-12** show the high acidic concentration Kalling

We utilized Kalling's No. 2 etching acid for this TIC and Alumina Powder specimens in this experiment via their formation of mixtures match of this specimens. Figure 3-13 show the high acidic concentration acid that we used in this process. Microstructure formation in high-chromium steels (more than 5% chromium) by an etching reagent. 5 g of copper chloride, 100 mL of hydrochloric acid, 100 mL of alcohol, and 100 mL of water make up the solution.

### **3.6.7 Optical Microscopy (OM)**

In addition to microbiology, microelectronics, nanophysics, biotechnology, and pharmaceutical research, optical microscopy is frequently employed in a variety of other fields of study. Histopathology, the study of biological specimens for medical diagnosis, can also be valuable. We definitely employed this optical microscope to see and determine a magnified picture of an item specimen with an objective lens and an eyepiece that amplified the image further so that we could observe it with the naked eye. Nanostructure refers to microstructure at scales smaller than can be observed with optical microscopes, whereas crystal structure refers to the arrangement of individual atoms. The ultrastructure of biological specimens is the nanostructure.

The influence of a microstructure on the mechanical and physical properties of a material is mostly determined by the presence or absence of certain flaws within the structure. These flaws can take several shapes, but pores are the most common. Even as pores have a significant part in defining the properties of a material, so does the material's composition.



**Figure 3-13 Optical Microscope**

### **3.6.8 Scanning Electron Microscope (SEM)**

A scanning electron microscope (SEM) is a type of electron microscope that generates images by scanning the surface of a specimen with a concentrated beam of electrons. Electrons interact with atoms in the sample, generating signals that carry information about the sample's surface topography and composition. The electron beam is scanned in a raster scan pattern, and the beam's position is coupled with the detected signal's intensity to create an image. It also employs a beam of relatively low-energy, focused electrons as an electron probe that is swept regularly across the material.

### **3.7 Equipment and Machine**

Robotic welding automates the welding process by utilising robots that execute and manage welding based on software that may be adjusted to match the requirements of the

project. Welders continue to supervise and monitor robotic welding, a more advanced form of automated welding in which machines perform the welding. So that the robot can control all processes, the system must be integrated with the robot, and the welding equipment must be compatible with and ideally designed for robotic welding.

### **3.7.1 ABB Robotic Welding IRB 1410**

The ABB Robotics model IRB 1410 is the one that we use for our project. The IRB 1410 offers rapid and reliable work cycles, which contribute to an increase in overall production. In applications involving arc welding, the robot has been utilized, and it has been demonstrated to deliver good performance and value, which has resulted in short payback times.

The robot's wrist has a capacity to handle 5 kilograms of weight, and its upper arm can support an additional 18 kilograms of weight for application-specific equipment. The exceptional levels of control and path precision that are required to ensure excellent work quality are necessary. Because you can change both the speed of the process and its position, you could achieve the highest possible level of manufacturing accuracy while simultaneously reducing or eliminating rejections. It is common knowledge that the IRB 1410 has a structure that is both solid and long-lasting. The benefits of this include low levels of noise, long intervals between routine maintenance, and a long-life span for the product. The robot's range of motion and reach allow it to operate over a large region. The wrist was slim, the design was compact, and the operation was high performance even in demanding and limited conditions.

The IRB 1410 features integrated wire feed wiring as well as mounting holes, allowing for the most efficient and effective assembly of process equipment on the arm.

Arc welding functions are included as standard in the IRC5 robot controller, and users can access these functions by using the FlexPendant, which is a patented device that serves as an interface for programming and operating the robot.

### 3.7.1.1 ABB Industrial Robot Control IRC5

The IRC5 is the industry standard for robot controller technology, based on more than four decades of robotics research and development. In addition to ABB's signature motion control, it features flexibility, safety, modularity, application interfaces, multi-robot control, and PC tool compatibility. The IRC5 is available in numerous configurations to provide optimal and cost-effective solutions for every application.

#### IRC5 Single Cabinet Controller

- Designed for high IP protection and full expandability
- Provides a protected environment for auxiliary equipment in the robot system
- MultiMove® opens previously unthinkable operations, thanks to the perfect coordination of complex motion patterns
- Capable of control of up to four robots in a MultiMove® setup. Just add a compact drive module to each additional robot



**Figure 3-14 IRC5 Single Cabinet Controller**

### 3.7.1.2 Kempfi KemArc Pulse 250

KempArc Pulse is a modular pulsed MIG/MAG welding automation system that offers productivity, adaptability, and a host of additional advantages. Combining robotic welding's dependable and consistent weld quality with KempArc Pulse's superior arc characteristics and rapid communication can take your production to a whole new level. Moreover, Kempfi Wise welding techniques can be fully utilised for automated welding. They increase efficiency in both thin-sheet and heavy-load applications. The analogue and digital versions of KempArc Pulse are compatible with a range of robotic control systems.



**Figure 3-15 Kempfi KemArc Pulse 250**

### 3.7.2 Milling Machine FM-16V8

With the appropriate attachments, the machine can be used for both vertical and horizontal milling, as well as milling various rotational surfaces and grooves, etc. It is the optimal machining equipment for the mechanical manufacturing, mould, vehicle, and motorbike sectors.

- Hardened and ground
- X axis auto feeding
- Y axis can be added auto feeding
- Milling head is driven by gear, can be used for drilling, milling, and tapping, easy and to operate.



**Figure 3-16 Milling Machine**

It is used to shape the workpiece by cutting slots, grooves, drilling, and performing all other operations involving shaping. The fundamental components of a milling machine include the base, column, arbor, knee, saddle, table, overhanging arm, elevating screw, and ram, among others. These components are responsible for the milling machine's proper operation. The workpiece is typically held in a vise or other similar device clamped to a table that can move in three perpendicular directions while the milling machine rotates the circular tool. Gears of all shapes and sizes can be machined on the milling machine. To create a slot or groove, it is most employed. It's capable of working on both flat and irregular surfaces, making it versatile. It is utilised in the manufacturing of complicated forms.

### 3.7.3 Wire Cut EDM Sodick VZ300L

In wire electrical discharge machining (WEDM), often referred to as wire-cut EDM and wire cutting, a thin single-strand metal wire, commonly brass, is fed through the workpiece, which is submerged in a tank of dielectric fluid, typically deionized water. It uses an electro thermal production technique in which a thin single-strand metal wire, together with de-ionized water (used to transmit electricity), enables the wire to cut through metal using heat from electrical sparks, while preventing rust.



**Figure 3-17 Sodick VZ300L wire-cut machine**

Figure 3-18 show the Wire-cut Sodick VZ300l machine that University Teknikal Malaysia Melaka provided us to operate and use it for this project. High performance LN2W generator ensures maximum speed and surface quality; spacious worktank with vertical access door. The end result is a high-performance machine with a wide range of possible uses. It makes it more simpler and more efficient to do this assignment.

### 3.7.4 Optical Microscope

Structures at the micro level are known as microstructure. Specifically, these are the structures of an item, organism, or material exposed by a microscope at magnifications greater than 25 times. flaws, impurities, and grains are commonly referred to as the microstructure when discussing a material's microstructure. The microstructure of a material (such as metals, polymers, ceramics, or composites) can have a significant impact on its physical properties, including strength, toughness, ductility, hardness, corrosion resistance, high/low temperature behavior, and wear resistance.



**Figure 3-18 Optical Microscope**

Microstructure. Only a microscope can reveal information about microstructure (stereo microscope, light microscope using reflected light, digital microscope or scanning and transmission electron microscope). From millimeters to micrometers and even nanometers, the typical size of characteristics seen is usually in the millimeter range.

Almost always, microstructures are produced when a material undergoes a phase shift caused by a change in temperature and/or pressure (e.g., a melt crystallization to a solid on cooling). Microstructures can be produced through deformation or material processing (e.g., rolling, pressing, welding). A material's microstructure can affect its physical qualities, such as corrosion resistance, strength, toughness, ductility, and hardness. These qualities contribute to the determination of the material's performance in a certain application.

### **3.7.5 Scanning Electron Microscope JEOL JSM-6010PLUS/LV**

A scanning electron microscope (SEM) is a type of electron microscope that generates images by scanning the surface of a specimen with a concentrated beam of electrons. Electrons interact with atoms in the sample, generating signals that carry information about the sample's surface topography and composition. The electron beam is scanned in a raster scan pattern, and the beam's position is coupled with the detected signal's intensity to create an image. Figure 3-20 show JEOL JSM-6010PLUS/LV SEM machine in UTeM FKM faculty.



**Figure 3-19 JEOL JSM-6010PLUS/LV SEM machine**

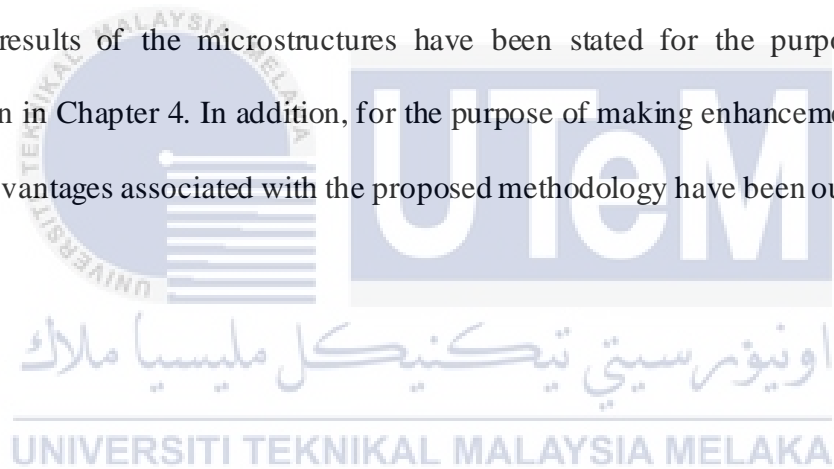
In this study, a JEOL JSM-6010PLUS/LV scanning electron microscope was utilised. This equipment provided scanning electron microscopy its resolving power, which is the finest detail a microscope can "see" or "resolve." Because the wavelength of the probing beam is orders of magnitude less than that of an optical microscope, the resolving power of electron microscopes is orders of magnitude greater than that of an optical microscope. The resolving power of a microscope is inversely proportional to the radiation or particle wave length composing the probe. Due to the fact that electrons have significantly shorter wavelengths than light, SEM can resolve finer features of specimens. A SEM has a far greater depth of focus than an optical microscope. Depth of focus is the capacity of a microscope to bring into focus the characteristics of an item at various depths.

### **3.8 Summary**

The methodology that has been proposed to develop the procedure for determining the effect of microstructure on ER308LSI in waam structure is described in this chapter.

The Gantt Chart will serve as the planning guide for the entire study, beginning at the very beginning and continuing all the way through to the very end. Additionally, a flowchart that illustrates the order in which the process to finish this study should be carried out has been developed.

This chapter has outlined the steps that need to be taken in order to complete the process as a whole. Aside from that, we will explain how we determine which of our parameters are most appropriate for this process. It took an excessive amount of time because we had to try and error on all of the parameters that we listed in order to get the exact parameter. In conclusion, the results of the time versus temperature analysis as well as the 50 results of the microstructures have been stated for the purpose of further investigation in Chapter 4. In addition, for the purpose of making enhancements, a number of the disadvantages associated with the proposed methodology have been outlined.



## CHAPTER 4

### 4.1 Introduction

This section describes the results and findings of a research into the effect of the microstructure on Stainless Steel ER308LSI arc wire that has been mixed with Titanium Carbide (TIC) and Alumina Oxide Powder. Optical Microscope data and an analysis of the microstructures of the blades will be displayed initially. Following that, a study of the characteristics of TIC and Alumina powder grains will be presented. Ultimately, it will present all data related to the microstructure effect. It is possible to add data from a literature review to this chapter in order to strengthen the explanation of every simulation outcome for both the base suspension system and the enhanced suspension system.

### 4.2 Surface Morphology of Walls

Figure 9 shows the surface morphology of titanium carbide (TIC) and alumina oxide walls. This image demonstrates that the surfaces of both processes exhibit a metallic sheen and periodic concave and convex contours due to layer-by-layer buildup. The contour and surface of the alumina oxide powder wall are more homogeneous and consistent. This is because the interaction between the stainless-steel arc and alumina oxide paste settles down the arc and creates a more homogenous molten pool. Each alumina oxide wall has a layer height of 7.2 0.3 mm and a layer thickness of 0.9 0.1 mm, whereas each titanium carbide wall has a layer height of 8.1 0.3 mm and a layer thickness of 0.9 0.1 mm. Because alumina oxide is a ceramic of chemical composition, this is the case. With the addition of Al<sub>2</sub>O<sub>3</sub> to er3081 si wire feeding, the heat input of each wire was drastically reduced, as was the size of the resulting weld pool. Therefore, for a wall with the same

desired thickness, the total feeding speed of alumina oxide powder is the same as that of titanium carbide powder, resulting in a faster stacking speed and greater efficiency.



**Figure 4-1 Surface morphology of alumina oxide powder left side, and titanium carbide powder right side**

### 4.3 Porosity of Walls

Porosity can produce stress concentration and lower the effective stressed area, which has a substantial impact on the performance of stainless steel. Figure 4-2 shows depicts the distribution of pores within alumina oxide and titanium carbide walls. Figure 4-2 reveals that the titanium carbide wall includes a considerable number of pores between 50 and 100 microns in diameter, which are primarily between layers (Figure 4-2). The number of pores in the alumina oxide wall reduced and the estimated diameter is 50 microns.

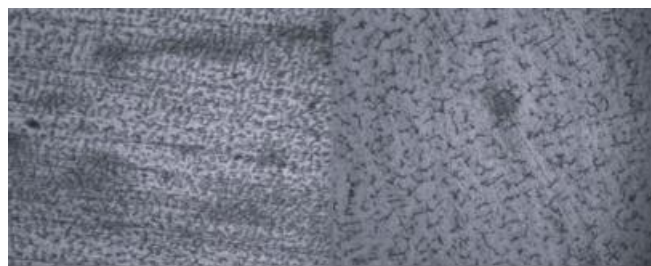


**Figure 4-2 Porosity of titanium carbide at the left side and the right side are the porosity of alumina powder wall.**

## 4.4 Microstructure of Walls

### 4.4.1 Microstructure of Walls in As-Deposited State

Figure 4-3 shows the microstructure of a stainless-steel wall in its as-deposited state. This is the standard microstructure stainless steel with austenite and twin grains. As seen in Figure 4-3a, the grains of the alumina oxide wall are composed mainly of isometric crystals with a tiny proportion of columnar crystals. The direction length of columnar crystals is parallel to the direction of growth of the wall, which is regulated by temperature and element gradient. As can be seen in Figure 4-3b, the titanium carbide grains make up the wall as isometric crystals. Grain size has been drastically decreased, and consistency has been enhanced. Heat input and percentage mixing paste that combine into stainless steel arc wire are the same, however the microstructure of the alumina oxide wall and the titanium carbide wall are different because of the quantity of wire feeding. As a result, isometric crystals form in the alumina oxide and titanium carbide, giving the walls a much greater degree of strength than would be possible with just stainless steel.

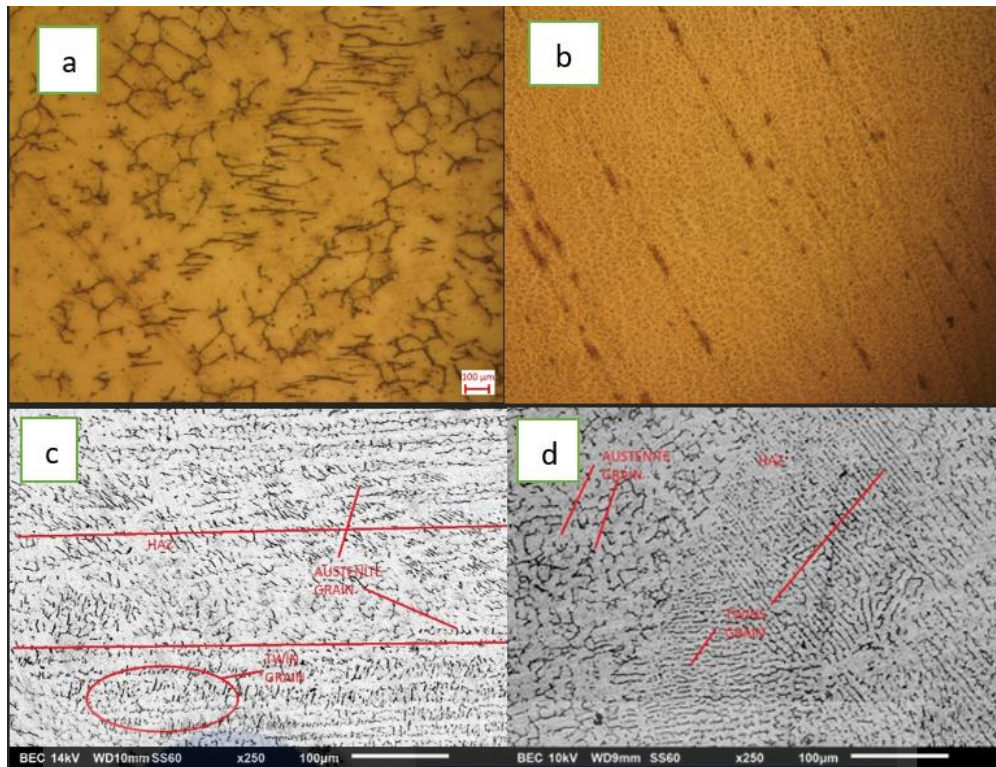


**Figure 4-3 Metallographs of (a) stainless steel wall and (b) alumina oxide wall, and SEM images of (C) titanium carbide wall and (D) alumina oxide wall in as-deposited state respectively.**

As can be shown in Figure 4c,d, the types of precipitated phases in the as-deposited states of alumina oxide and titanium carbide walls were consistent, with T phase and phase as the predominant ones. Compared to the alumina oxide wall, the precipitated phase of the titanium oxide wall is more equally distributed in the grains or on the grain border. This is due to the strengthens relatively from stainless steel wall and that the solubility of manganese sulphides is much higher than that in the solid state, so the content of manganese sulphides in the later solidified alumina carbide and titanium carbide wall is higher and the size of the precipitated  $\theta$  phase is larger with little segregation.

## 4.5 Mechanical Properties and Fracture Morphology of Walls

### 4.5.1 Mechanical Properties of Walls

Figure 4-4 displays the mechanical characteristics of walls made of alumina oxide and titanium carbide following the waam process. The numbers 1 and 2 here stand for the mechanical properties of the element compounds making up the titanium carbide wall, whereas the numbers 3 and 4 stand for the element compounds making up the alumina oxide wall. As can be observed in Figure 4-4, the small amount of powder used (0.5 milligrams) significantly reduces the mechanical characteristics of titanium carbide and alumina oxide. Because we make a paste and put it in the bead during the waam process at temperatures below 150 degrees Celsius, the amount of titanium carbide and alumina oxide is too small for the EDX machine to detect its existence. However, we have already found out the differences of the microstructure of the inoculant and this is made possible through the use of tensile stress.

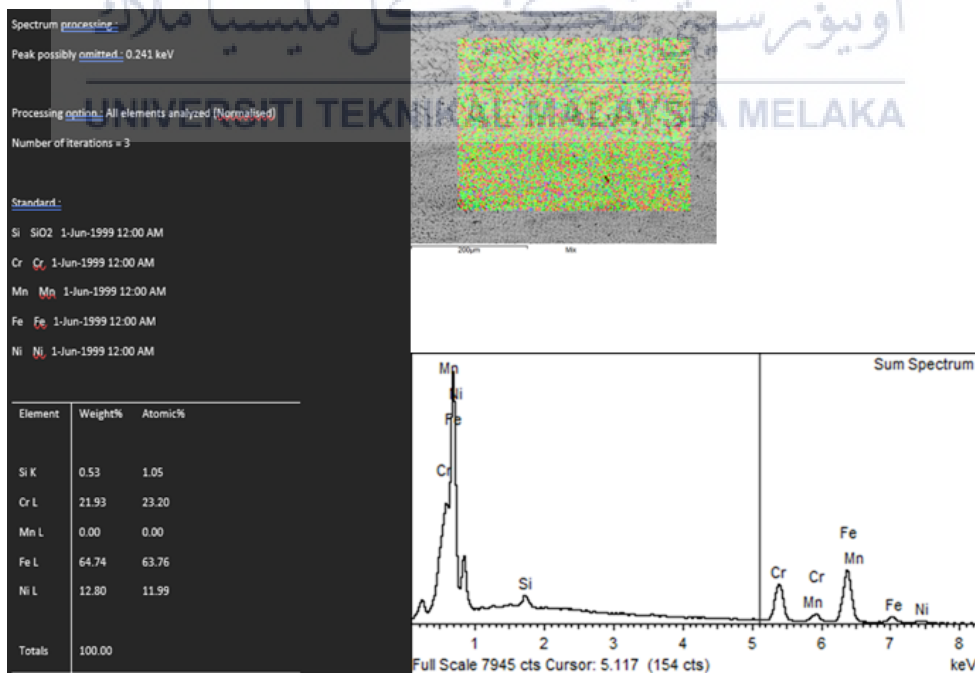
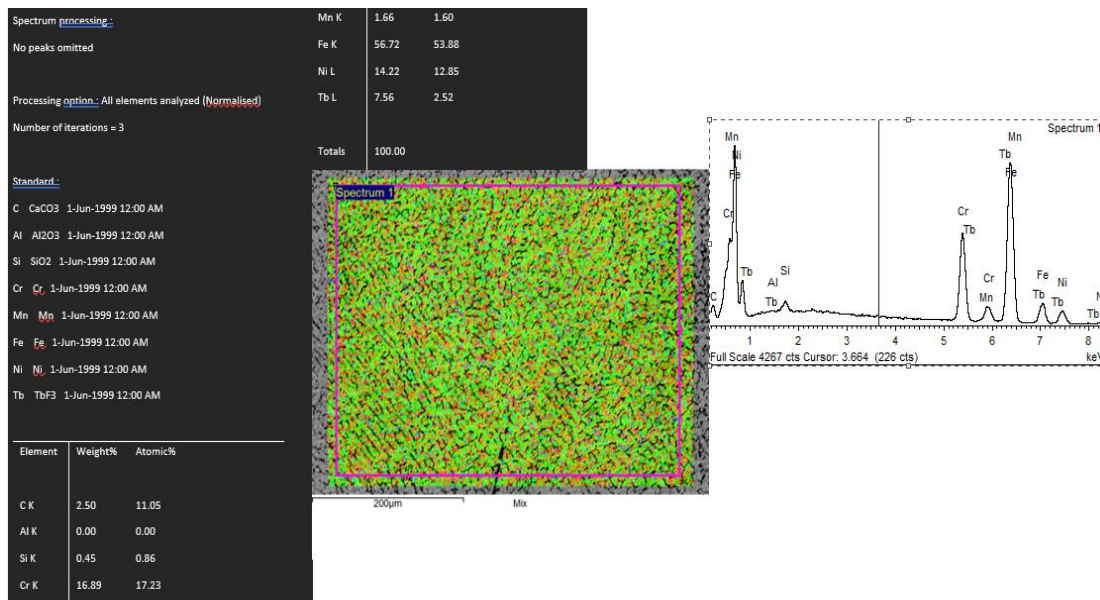


Figure 4-4 Mechanical properties of printed Titanium Carbide wall



**Figure 4-5 Mechanical properties of printed Alumina oxide wall**

#### 4.5.2 Fracture Morphology of Walls

Figure 4-6 depicts the fracture morphologies of alumina oxide (a and b) and titanium carbide (c and d) wall materials from different directions. In Figure 4-6, it is clear that the fracture mode is "an intercrystalline brittle fracture, as the morphology of longitudinal fractures in the titanium oxide wall consists of several cleavage planes with only a few shallow dimples. It is clear that a mixed-fracture process is at work here, as the transverse fracture of the alumina oxide wall consists of both cleavage planes and dimples. This is mainly due to the presence of unresolved phases on the grain boundary after heat treatment, which reduces the toughness of the stainless steel and acts as a fracture initiation source. The fracture mechanism of the alloy is ductile fracture, thus the double-wire wall has great strength and toughness. Fractures in the titanium carbide wall, both longitudinal and transverse, are filled by a large number of dimples of uniform size.

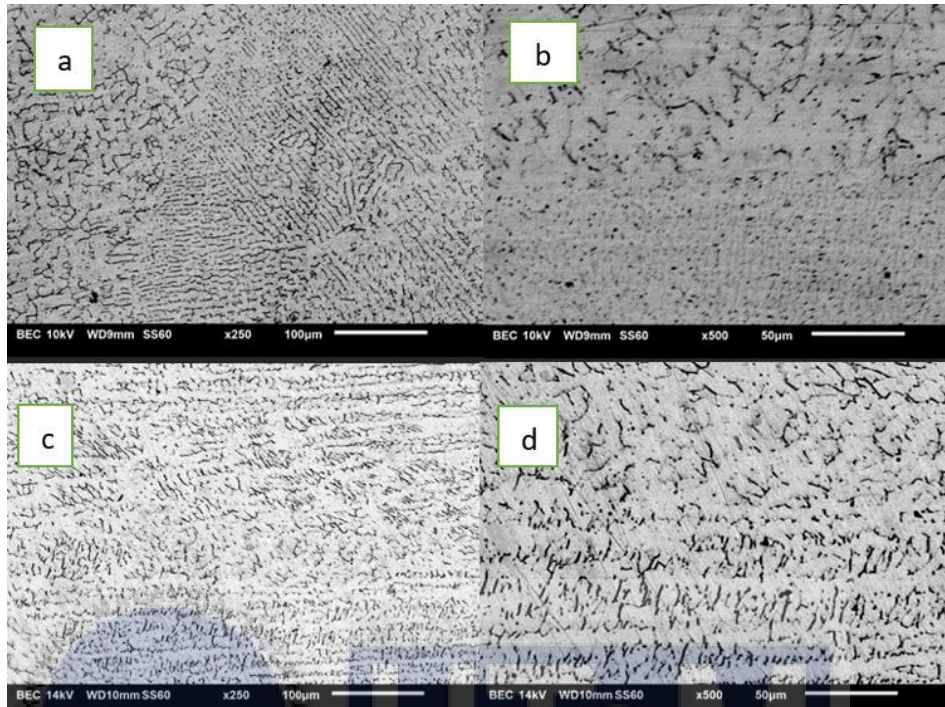


**Figure 4-6 SEM images showing fracture morphology of alumina oxide and titanium carbide: (A) longitudinal of alumina oxide; (b) transverse of alumina oxide; (c) longitudinal of titanium carbide; and (d) transverse of titanium carbide.**

## CHAPTER 5

### 5.1 Conclusions

In this work, stainless steel ER308L Si walls were produced utilizing the WAAM method with paste mixtures from the alumina oxide and titanium carbide procedures. Surface shape, microstructure as deposited, and mechanical properties, respectively. Examining the mechanical characteristics, surface morphology, and microstructure of the as-deposited were all done. These inferences are made:

- i) The surface quality of the wall and the accumulation efficiency both increased despite the fact that the wire feeding speed remained unchanged and the amount of heat input and alumina oxide and titanium carbide paste remained unchanged.
- ii) When alumina oxide powder is combined with stainless steel arc wire, the resulting microstructure of the resulting grains is identical to that of the stainless-steel wall.
- iii) The microstructure is similar to that of stainless steel, but the combined strength of alumina carbide and titanium oxide makes the material far more formidable than stainless steel alone.

### 5.2 Recommendation

Based on findings and conclusion of the study, here are several recommendations to be considered for future research:

- In order to make a stronger specimen, it is recommended to add alumina oxide powder and titanium carbide powder to the paste prior to beginning the waam process.
- Impact the world by analysing the structural differences between the walls of stainless steel, alumina oxide, and titanium carbide.
- Utilizing the tig welding technique and etching that is suitable with the material generated to achieve meaningful results.



## REFERENCES

- Arc, W. (n.d.). *WAAM Education Cell*.
- Bilbao, J., & Lamikiz, A. (2020). *High deposition wire arc additive manufacturing of mild steel : Strategies and heat input effect on microstructure and mechanical properties*. 58(June), 615–626. <https://doi.org/10.1016/j.jmapro.2020.08.060>
- Jin, P., Liu, Y., Li, F., & Sun, Q. (2021). Realization of synergistic enhancement for fracture strength and ductility by adding TiC particles in wire and arc additive manufacturing 2219 aluminium alloy. *Composites Part B: Engineering*, 219(2), 108921. <https://doi.org/10.1016/j.compositesb.2021.108921>
- Khalid, N., Zirwatul, P., Zamanhuri, N. M., Ahmad, F., & Baharin, S. (2017). *A STUDY OF WELD DEFECTS OF GAS METAL ARC WELDING WITH DIFFERENT SHIELDING GASSES*. 12(6), 2006–2011.
- Le, V. T., Mai, D. S., Doan, T. K., & Paris, H. (2021). Wire and arc additive manufacturing of 308L stainless steel components: Optimization of processing parameters and material properties. *Engineering Science and Technology, an International Journal*, 24(4), 1015–1026. <https://doi.org/10.1016/j.jestch.2021.01.009>
- Le, V. T., Mai, D. S., & Hoang, Q. H. (2020). A study on wire and arc additive manufacturing of low-carbon steel components: process stability, microstructural and mechanical properties. *Journal of the Brazilian Society of Mechanical Sciences and Engineering*, 42(9). <https://doi.org/10.1007/s40430-020-02567-0>
- Liew, J., Li, Z., Alkahari, M. R., Ana, N., Rosli, B., & Hasan, R. (2019). *Review of Wire Arc Additive Manufacturing for 3D Metal Printing*. 13(3).
- Nallusamy, T., & S, V. (2021). High-Temperature Stability of Titanium Boride Reinforced Alumina-Silicon Carbide Based Composite. *Silicon*, 13(4), 1087–1095. <https://doi.org/10.1007/s12633-020-00498-y>
- Rafieazad, M., Ghaffari, M., Vahedi Nemani, A., & Nasiri, A. (2019). Microstructural evolution and mechanical properties of a low-carbon low-alloy steel produced by wire arc additive manufacturing. *International Journal of Advanced Manufacturing Technology*, 105(5–6), 2121–2134. <https://doi.org/10.1007/s00170-019-04393-8>
- Ron, T., Levy, G. K., Dolev, O., Leon, A., Shirizly, A., & Aghion, E. (2019). Environmental behavior of low carbon steel produced by a wire arc additive manufacturing process. *Metals*, 9(8). <https://doi.org/10.3390/met9080888>

- Wu, B., Ding, D., Pan, Z., Cuiuri, D., Li, H., Han, J., & Fei, Z. (2017). Effects of heat accumulation on the arc characteristics and metal transfer behavior in Wire Arc Additive Manufacturing of Ti6Al4V. *Journal of Materials Processing Technology*, 250, 304–312. <https://doi.org/10.1016/j.jmatprotec.2017.07.037>
- Yuan, L., Pan, Z., Ding, D., He, F., van Duin, S., Li, H., & Li, W. (2020). Investigation of humping phenomenon for the multi-directional robotic wire and arc additive manufacturing. *Robotics and Computer-Integrated Manufacturing*, 63(July 2019), 101916. <https://doi.org/10.1016/j.rcim.2019.101916>



## FAKULTI TEKNOLOGI KEJURUTERAAN MEKANIKAL DAN PEMBUATAN

Tel : +606 270 1184 | Faks : +606 270 1064

Rujukan Kami (Our Ref):  
Rujukan Tuan (Your Ref):  
Tarikh (Date): 31 Januari 2021

Chief Information Officer  
Perpustakaan Laman Hikmah  
Universiti Teknikal Malaysia Melaka

Melalui

Dekan  
Fakulti Teknologi Kejuruteraan Mekanikal dan Pembuatan  
Universiti Teknikal Malaysia Melaka

Tuan

### PENKELASAN TESIS SEBAGAI TERHAD BAGI TESIS PROJEK SARJANA MUDA

Dengan segala hormatnya merujuk kepada perkara di atas.

2. Dengan ini, dimaklumkan permohonan pengkelasan tesis yang dilampirkan sebagai TIDAK TERHAD untuk tempoh **LIMA** tahun dari tarikh surat ini. Butiran lanjut laporan PSM tersebut adalah seperti berikut:

**Nama pelajar: SHAHRUL HELMI BIN LASEMIN**

**Tajuk Tesis: The effect of microstructure onto ER308L Si WAAM structure using inoculant.**

3. Hal ini adalah kerana IANYA MERUPAKAN PROJEK YANG BUKAN DITAJA OLEH SYARIKAT LUAR DAN HASIL KAJIANNYA ADALAH TIDAK SULIT.

Sekian, terima kasih.

**“BERKHIDMAT UNTUK NEGARA”**  
**“KOMPETENSI TERAS KEGEMILANGAN”**

Saya yang menjalankan amanah,



**TS. MOHD HAIRIZAL BIN OSMAN**

Pensyarah Kanan  
Jabatan Teknologi Industri  
Fakulti Teknologi Kejuruteraan Mekanikal dan Pembuatan  
Universiti Teknikal Malaysia Melaka

SEBUAH UNIVERSITI TEKNIKAL AWAM



CERTIFIED TO ISO 9001:2015  
CERT. NO. : QMS 01385